MUM: Flexible precise Monte Carlo algorithm for muon propagation through thick layers of matter

Igor A. Sokalski, Edgar V. Bugaev, and Sergey I. Klimushin
Institute for Nuclear Research, Russian Academy of Science, 60th October Anniversary Prospect 7a, Moscow 117312, Russia
(Received 9 December 2000; revised manuscript received 13 June 2001; published 10 September 2001)

We present a new Monte Carlo muon propagation algorithm MUM (muons+medium) which possesses some advantages over analogous algorithms presently in use. The most important features of this algorithm are described. The results on the test for the accuracy of the treatment of the muon energy loss with MUM are presented and analyzed. It is evaluated to be of 2×10^{-3} or better, depending upon simulation parameters. The contributions of different simplifications, which are applied at Monte Carlo muon transportation to the resulting error, are considered and ranked. It is shown that when simulating muon propagation through a medium it is quite enough to account only for fluctuations in radiative energy loss with the fraction of energy lost being as large as $>0.05-0.1$. Selected results obtained with MUM are given and compared with ones from other algorithms.

DOI: 10.1103/PhysRevD.64.074015 PACS number(s): 13.85.Tp, 96.40.Tv

I. INTRODUCTION

Muon propagation through thick layers of matter has been in the scope of interest for a long time, since the first underground experiments with natural muon and neutrino fluxes began. The development of the ''underground'' technique has led to the creation of a number of underground, underwater, and under-ice detectors by which a wide spectrum of problems are presently under investigation. An accurate calculation of the muon transport plays an important role for such experiments because (a) neutrinos are detected by muons that are born in νN interactions and propagate a distance in medium from the point of interaction to a detector; (b) muons that are produced in atmospheric showers generated by cosmic rays represent the principal background for a neutrino signal and therefore their flux at large depths should be well known; (c) atmospheric muons deep under the sea or the Earth's surface are the only intensive and more or less known natural calibration source, which allows one to confirm the correctness of the detector model by the comparison of the experimental and expected detector response; and (d) the flux of atmospheric muons itself carries the physical information which is of interest.

Along with analytical and semianalytical methods (Refs. [1–13]) one widely uses the Monte Carlo (MC) technique (Refs. [14–25]) which directly accounts for the stochastic nature of muon energy losses to simulate the muon propagation through matter. There are several MC muon transportation algorithms currently in use (see, e.g., Ref. [26] for a detailed analysis of their advantages and disadvantages) but essential theoretical and experimental progress of last years makes to create new ones. Here we present a MC muon propagation code MUM (muons+medium) written in FORTRAN, which possesses some advantages in accuracy and flexibility over analogous simulation algorithms (although it does not contain some important features in its current version, e.g., it does not give the three-dimensional information about angular and lateral deviations of muons). The algorithm has been developed for the Baikal deep underwater neutrino experiment (Ref. [27]) but we believe it to also be useful for other experiments with natural fluxes of high-energy muons and neutrinos. When working on MUM we aimed at the creation of an algorithm that would (a) account for the most recent corrections for the muon cross sections; (b) be of adequate and known accuracy, i.e., not contribute an additional systematic error, which would exceed one from ''insurmountable'' uncertainties (e.g., with muon and neutrino spectra and cross sections) and whose value would be well known for any setting of simulation parameters; (c) be flexible enough, i.e., could be optimized for each concrete purpose to desirable and well-understood equilibrium between computation time and accuracy, and be easily extended for any medium and any correction for the cross sections of the processes in which high-energy muon loses its energy; (d) be ''transparent,'' i.e., provide the user with the whole set of data related to used models for the muon cross sections; and (e) be as fast as possible.

We describe the main features of our algorithm in Sec. II. Section III gives an analysis for the algorithm accuracy. In Sec. IV we report the results of the investigation on the set of parameters that should be used to simulate the muon propagation with an optimum equilibrium between accuracy and computation time. Section V presents selected results obtained with MUM in comparison with ones from other muon propagation MC codes, namely, PROPMU (Ref. [22]) and MUSIC (Ref. [24]). Section VI gives general conclusions. We also present parametrizations for muon cross sections as they are used in MUM in Appendix A and give proof of a formula for the free path between two muon interactions, as treated in our algorithm, in Appendix B.

II. ALGORITHM DESCRIPTION

The basic features of the MUM algorithm are as follows.

(a) The code does not use any preliminary computed data as an input, all necessary tables are prepared at the stage of initiation on the base of five relatively short routines, four of which return differential cross sections $d\sigma(E,v)/dv$ (where E is muon energy, and v is fraction of energy lost v

$=\Delta E/E$) for bremsstrahlung, direct e^+e^--pair production, photonuclear interaction and knock-on electron production, correspondingly, and a fifth one that returns stopping power due to ionization $[dE(E)/dx]_{ion}$ (see Appendix A for corresponding formulas). Thus, it is easy for any user to correct or even entirely change the model for muon interactions, as it is necessary. Also, any material can be easily composed. Three media, namely, pure water, ice, and standard rock are available directly.

(b) We have tried to decrease the ''methodical'' part of the systematic error that originates from the finite accuracy of the numerical procedures on interpolation, integration, etc., down to as low a level as possible, and special attention was put on procedures that simulate the free path between two sequential muon interactions and the fraction of energy lost. To combine this with the high speed of simulation, the values for free paths, energy losses, and differential and total cross sections, along with solutions for all ordinary and integral equations, are computed in MUM at the initiation stage, tabulated, and then referenced when necessary with an interpolation algorithm whose accuracy has been carefully tested for each table by comparison with directly computed values to be not worse than 0.5% (typically, much better).

(c) The most important parameters are changeable and can be tuned to an optimum combination, depending upon desirable accuracy, necessary statistics, and restriction on the computation time for each concrete problem.

(d) The code combines algorithms for muon transportation through thick layers of matter down to the detector and for simulation muon interactions within detector sensitive volume (these algorithms have to differ from each other). This is important for deep underwater and under-ice Cherenkov neutrino telescopes (see Refs. [27–30]), where the same material (water or ice) represents both a shield that absorbs atmospheric muons and detecting medium in which muons and shower particles, resulting from muon interactions, generate Cherenkov photons detected by phototubes.

(e) Formally, initial muon energies up to 1 EeV can be processed by the MUM algorithm, but uncertainties with muon cross sections, which grow along with the muon energy (especially, for photonuclear interaction) causes one to apply the MUM output with care at muon energies $E>1$ PeV.

(d) Besides the muon transportation algorithm itself, the code includes a number of routines that allow us to obtain values for differential and total cross sections, mean free paths, energy losses and other related data for the given set of input parameters directly. Sampling the atmospheric muon energies at the sea level according to the different models for the spectrum is possible with MUM, as well. Also several test procedures are included that provide data concerning the accuracy of different algorithm steps. See Sec. III, Sec. IV, and Sec. V for the selected output of these procedures.

The usual approximation for the treatment of the muon energy loss is applied in the MUM algorithm; muon interactions with comparatively large energy transfers when a fraction of energy lost v exceeds some value v_{cut}, are accounted for by the direct simulation of $v \geqslant v_{cut}$ for each single interaction, according to the shape of differential cross sections [these interactions lead to ''stochastic'' energy loss (SEL)] while the part of the interaction with relatively small v is treated by the approximate concept of ''continuous'' energy loss (CEL) using the stopping power formula

$$\left[\frac{dE}{dx}(E)\right]_{CEL} = \frac{N_A}{A_{eff}}\rho E \sum_{j=b,p,n}\sum_{i=1}^{n}\left[k_i \int_{v_{min}^{i,j}}^{v_{cut}} \frac{d\sigma_i^j(E,v)}{dv} v\, dv\right] + \left[\frac{dE}{dx}(E)\right]_{ion} - \frac{N_A}{A_{eff}}\rho E \sum_{i=1}^{n}\left[k_i \int_{v_{cut}}^{v_{max}^{i,e}} \frac{d\sigma_i^e(E,v)}{dv} v\, dv\right]. \tag{2.1}$$

Here the index j indicates the type of interaction ($j=b$ for bremsstrahlung, $j=p$ for direct e^+e^--pair production, $j=n$ for photonuclear interaction, and $j=e$ for knock-on electron production, respectively); index i runs over n kinds of atoms which given material consists of; $k_i=N_i/N_{tot}$ is a fraction of the ith element; N_i and N_{tot} are the number of a given kind of atoms and the total number of atoms, respectively, per unit of material volume; N_A is the Avogadro number; ρ is the material density; $A_{eff}=N_{tot}^{-1}\Sigma_{i=1}^{n}(N_iA_i)$ is an effective atomic weight for a given material; A_i is atomic weight for the ith element; $v_{min}^{i,j}$ is the minimum kinematically allowed fraction of energy lost for the ith element at the jth process. One is forced to decompose energy losses into two parts because the simulation of all interactions with $v \geqslant v_{min}$ would result in infinite computation time due to the steep dependence of muon cross sections on v: they decrease with v at least as $d\sigma(E,v)/dv \propto v^{-1}$, and for some processes are not finite at $v \to 0$. The number of interactions to be simulated per unit of muon path grows, roughly, as $N_{int} \propto v_{cut}^{-1}$ along with the computation time. Actually, two different criteria by which the given muon interaction is attributed either to SEL or to CEL, are available in the frame of the MUM algorithm. The first one (relative) has been described above and is applied when the muon is transported down to the detector location. Second, absolute criterium, is useful when simulating muon interactions within an underwater or under-ice array to obtain the detector response with the fixed energy threshold; interaction is of SEL type if $\Delta E \geqslant \Delta E_{cut}$ and of CEL type, if $\Delta E < \Delta E_{cut}$. Optionally, the cross section for the knock-on electron production $d\sigma^e(E,v)/dv$ can be set in MUM to zero, in which case muon propagation down to the detector is simulated with entirely ''continuous'' ionization and its fluctuations are neglected, but the simulation of the muon interactions with the fixed energy threshold includes knock-on electron production in any case. Both v_{cut} and ΔE_{cut} represent parameters for the MUM initiation procedure and can be set to any values within $10^{-4} \leqslant v_{cut} \leqslant 0.2$ and 10 MeV$\leqslant \Delta E_{cut} \leqslant$500 MeV, correspondingly. The optimum value for ΔE_{cut} depends upon the configuration of the given detector and also upon characteristics of algorithms that simulate the shower development, the Cherenkov photons generation and the propagation, and the detector response. All this is out of this article's scope, therefore we do

not discuss this parameter below, except for mentioning that Eqs. (2.1), (2.3), and (2.6) are used in the algorithm with the absolute treatment of the muon energy loss decomposition being modified by replacement $v_{cut} \to \Delta E_{cut}/E$. The influence of the simplified entirely ''continuous'' treatment of the ionization and value of v_{cut} upon the simulation accuracy is analyzed in detail in Sec. IV (see also Ref. [31]).

The principal steps of simulation are as follows.

(i) For a muon with initial energy E_1, the free path L until interaction with $v \geqslant v_{cut}$ is simulated. For this, after a random number η, uniformly distributed in a range from 0 to 1, has been sampled, one solves the following set of equations:

$$-\ln(\eta) = \int_{E_2}^{E_1} \{[dE(E)/dx]_{CEL} \overline{L}(E)\}^{-1} dE,$$

$$L = \int_{E_2}^{E_1} \{[dE(E)/dx]_{CEL}\}^{-1} dE, \tag{2.2}$$

[the proof of Eqs. (2.2) is given in Appendix B]. Here, $E_2 < E_1$ is the muon energy at the point of interaction and the energy dependent mean-free-path $\overline{L}(E)$ between two interactions with the fraction of energy lost $v \geqslant v_{cut}$, is expressed by

$$\overline{L}(E) = \frac{A_{eff}}{\rho N_A} \left\{ \sum_{j=b,p,n,e} \sum_{i=1}^{n} \left[k_i \int_{v_{cut}}^{v_{max}^{i,j}} \frac{d\sigma_i^j(E,v)}{dv} dv \right] \right\}^{-1}, \tag{2.3}$$

where $v_{max}^{i,j}$ is the maximum kinematically allowed fraction of energy lost for the ith element at the jth kind of interaction. The first equation in Eqs. (2.2) is solved for the variable E_2, then the free path L can be found by a second equation. We would like to stress that such an approach allows us to perform the accurate simulation independently on the chosen value of v_{cut}, in contrast to the commonly used simplification

$$L_{approx} = -\overline{L}(E_1)\ln(\eta), \tag{2.4}$$

which neglects dependence $\overline{L}(E)$ upon energy and, consequently is (a) less accurate the larger v_{cut} is, and (b) produces the error of different signs for the cases when the ionization is included in SEL or its fluctuations are neglected. It is illustrated by two plots in Fig. 1. The upper plot shows the function $\overline{L}(E)$ for pure water. Two sets of curves are presented for two models of ionization. Each set includes dependencies for three values of v_{cut}: 10^{-4}, 10^{-3}, and 10^{-2}. In fact, $\overline{L}(E)$ is almost a constant at $E > 5$ TeV, but changes steeply at lower energies. It increases with the decrease of energy if the ionization is entirely ''continuous'' and, on the contrary, it decreases if the ionization is included in SEL. Thus, by simulating the free path by Eq. (2.4) one overestimates it (and consequently underestimates the energy loss) in the case when ionization is included in SEL and, on the contrary, one underestimates the free path and overestimates the energy loss in the case of completely ''continuous'' ionization. The lower plot in Fig. 1 shows the resulting error

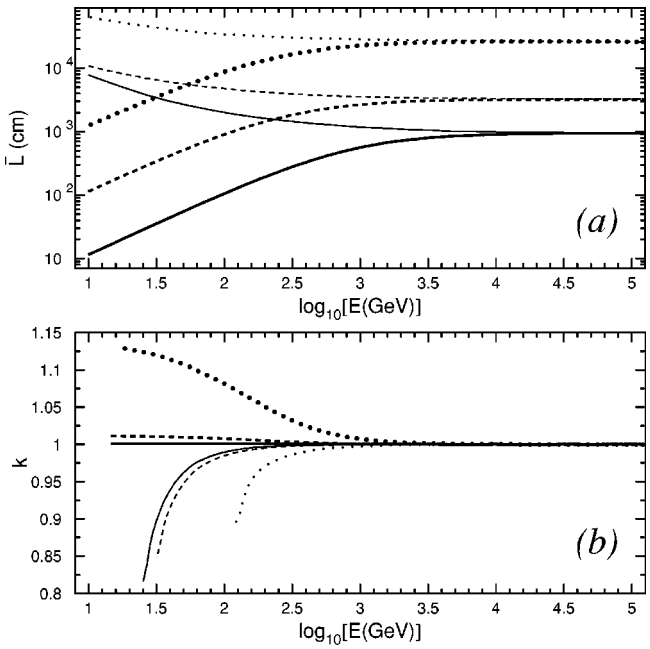

FIG. 1. (a) The mean-free-path between two sequential muon interactions with the fraction of energy lost $v \geqslant v_{cut}$ $\overline{L}(E)$ [Eq. (2.3)] in pure water vs muon energy. Two sets of curves correspond to two models of ionization. Thick lines are for ionization included in SEL, thin ones correspond to entirely ''continuous'' ionization. Solid lines: $v_{cut} = 10^{-4}$; dashed lines: $v_{cut} = 10^{-3}$; and dotted lines: $v_{cut} = 10^{-2}$. (b) Function $k(E) = L_{approx}(E)/L(E)$ for $-\ln(\eta) = 1$ (see text). The thickness and type of lines are of the same meaning as for plot (a).

in the value of the simulated free path, if $-\ln(\eta) = 1$ [for larger $-\ln(\eta)$ the effect is more significant]. The set of curves represent the dependencies $k(E) = L_{approx}(E)/L(E)$ with $L(E)$ computed by Eqs. (2.2) and $L_{approx}(E)$ computed by Eq. (2.4). With ionization included in SEL, overestimation for the free path is less than 1% at $v_{cut} \leqslant 10^{-3}$, but reaches $\sim 15\%$ at $v_{cut} = 10^{-2}$ which leads to 1–2% underestimation of total energy loss below the muon energy 1 TeV. In the case with ''continuous'' ionization, the effect is of the opposite sign and again is more significant for large v_{cut}.

(ii) After the free path L and the muon energy E_2 have been found from Eqs. (2.2), the type of interaction is simulated according to the proportion between the total cross sections of different processes:

$$\sigma^b : \sigma^p : \sigma^n : \sigma^e \tag{2.5}$$

which are computed as

$$\sigma^j = \sum_{i=1}^{n} \left[k_i \int_{v_{cut}}^{v_{max}^{i,j}} \frac{d\sigma_i^j(E_2,v)}{dv} dv \right]. \tag{2.6}$$

(iii) The fraction of energy lost v is simulated according to the shape of the differential cross section for a given process j:

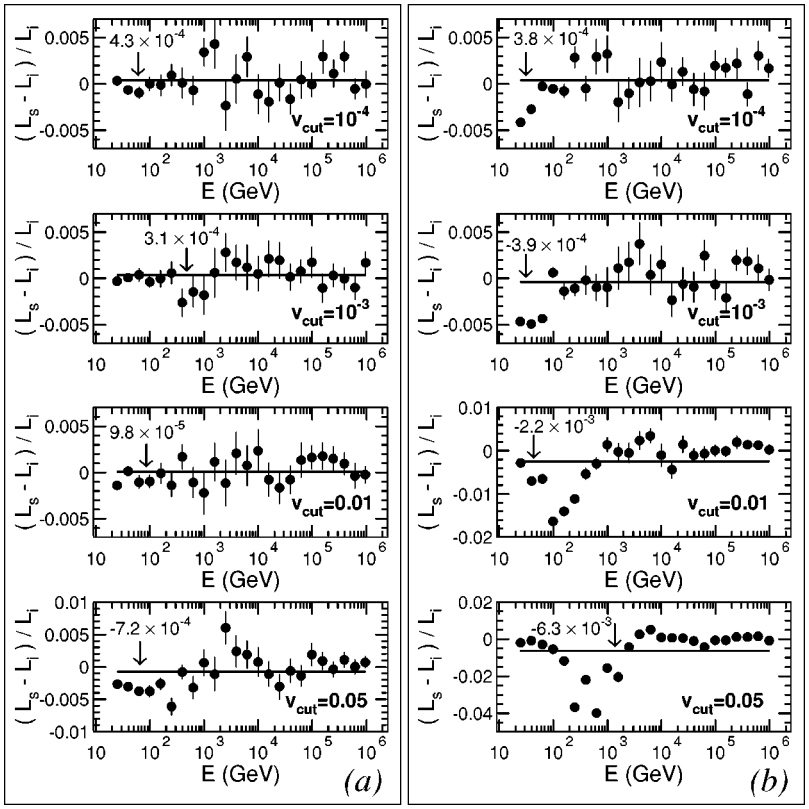

FIG. 2. The relative difference $(L_s-L_i)/L_i$ between "simulated" L_s [Eq. (3.1)] and "integrated" L_i [Eqs. (3.2),(3.3)] total muon energy loss in the pure water. The horizontal solid line on each plot shows the value for $(L_s-L_i)/L_i$, averaged over 24 tested muon energies which, additionally, is given in the upper-left corner of the figure. The statistical error at the 1σ level is shown at each point. (a)—Ionization is included in SEL; (b)—ionization is entirely "continuous."

$$\frac{d\sigma^j}{dv}(E_2,v)=\sum_{i=1}^{n} k_i \frac{d\sigma_i^j}{dv}(E_2,v) \tag{2.7}$$

and the new muon energy $E_1'=E_2(1-v)$ is determined.

(iv) Steps i–iii are repeated sequentially until the muon either reaches the level of observation or stops. A muon is considered stopped as soon as its energy decreases down to 0.16 GeV, which corresponds to the Cherenkov threshold for a muon in pure water.

III. ALGORITHM ACCURACY

As described in Sec. II, the MUM code (as well as any muon MC propagation algorithm) consists of the set of procedures on the numerical solution of equations, interpolation, and integration. All these procedures are of finite accuracy and, consequently, the incoming model for muon energy loss is somewhat corrupted by them. Thus, the resulting energy loss as *simulated* by a code is not the same as the energy loss as can be calculated by the *integration* of the differential cross sections, which are at the input of the same code. The difference between the simulated and calculated energy loss contains errors that are contributed by each step of simulation algorithm and thus, is a good quantitative criteria for its *inner accuracy*, whose contribution to the resulting error must not exceed one, which comes, e.g., from uncertainties with muons cross sections and medium composition. Therefore to demonstrate the accuracy of the presented algorithm, we have only chosen data on the relative difference $(L_s-L_i)/L_i$ between simulated L_s and integrated L_i total muon energy loss as was obtained with MUM for the pure water (Fig. 2) and standard rock ($\rho=2.65$ g cm^{-3}, $A=22$, $Z=11$, Fig. 3). Inner accuracy is presented in the figure as a function of muon energy for several values of v_{cut} and two models of ionization energy loss. Values of L_s were obtained as follows. For each muon energy E_1 a distance D was chosen and propagation of $N=4\times10^6$ muons over this distance was simulated. The condition $ND\gg\overline{L}(E_1)$ must be obeyed to obtain a statistically significant result but, at the same time, D should be short enough to be passed by muons without decreasing their energy down to zero, which practically leads to $D=0.5$ m–300 m, depending upon the muon energy, the value of v_{cut}, and the kind of medium. For each ith muon its final energy E_2^i was fixed and then L_s was calculated as

$$L_s=\frac{1}{D}\left(E_1-\frac{1}{N}\sum_{i=1}^{N} E_2^i\right). \tag{3.1}$$

L_i was computed as

$$L_i=\frac{1}{D}(E_1-E_2), \tag{3.2}$$

where E_2 was found as a solution of integral equation for the muon range:

$$D=\int_{E_2}^{E_1}\left\{\frac{N_A}{A_{eff}}\rho E\sum_{j=b,p,n}\sum_{i=1}^{n}\left[k_i\int_{v_{min}^{i,j}}^{v_{max}^{i,j}}\frac{d\sigma_i^j(E,v)}{dv}v\,dv\right]+\left[\frac{dE}{dx}(E)\right]_{ion}\right\}^{-1}dE. \tag{3.3}$$

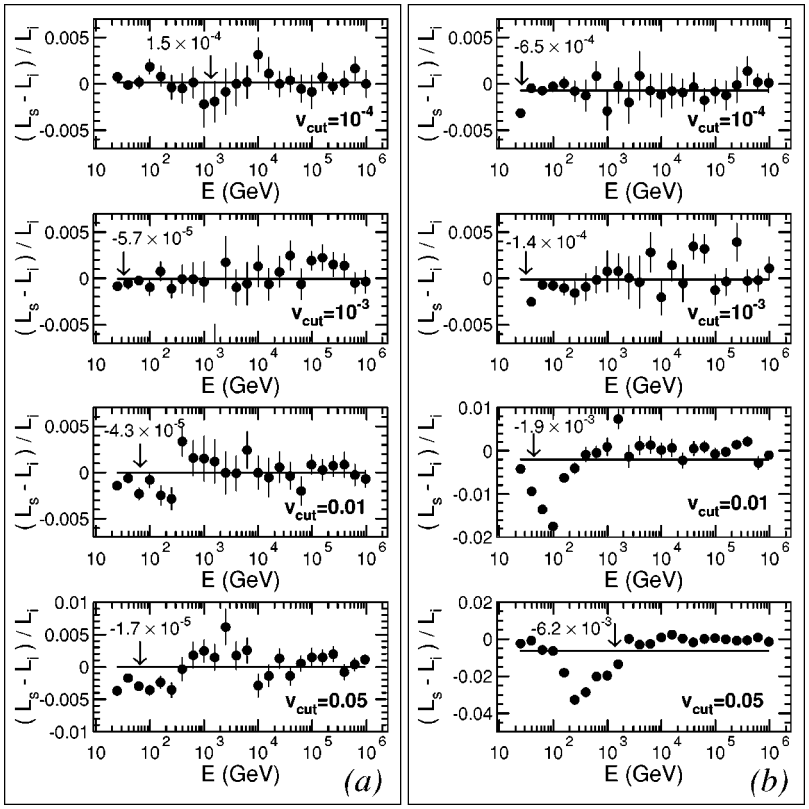

FIG. 3. The same as in Fig. 2 for standard rock ($\rho=2.65$ g cm^{-3}, $A=22$, $Z=11$).

The horizontal solid line on each plot shows the value for $(L_s-L_i)/L_i$ averaged over 24 tested muon energies, which, additionally, is given in the upper-left corner of the figure. Figures 2(a) and Fig. 3(a) indicate an excellent inner accuracy of the MUM algorithm with ionization included in SEL, both for water and standard rock. Up to $v_{cut}=5\times10^{-2}$ all points are within 0.6% deviations, which are of both signs, so the averaged accuracy remains better than 10^{-3}. Figures 2(b) and Fig. 3(b) (which correspond to simplified completely ''continuous'' ionization) shows a somewhat worse accuracy of the algorithm that falls down when v_{cut} increases. The accuracy was found to be within 1% (except for a few points around muon energy $E=100$ GeV) up to $v_{cut}=10^{-2}$ with averaged accuracy within 2×10^{-3}. This last value may be used as a conservative evaluation of the inner accuracy for the MUM algorithm. Statistically significant likeness of plots obtained for water and standard rock can be seen.

Thus, we conclude that assuming an optimistic evaluation of 1% for uncertainties in muon cross sections (Refs. [26,32]) the inner inaccuracy of MUM does not exceed them for any $v_{cut}\leqslant 5\times10^{-2}$ if ionization is included in SEL, and for any $v_{cut}\leqslant 10^{-2}$ if ionization is treated as entirely ''continuous process,'' independently of material.

IV. THE OPTIMUM SETTING OF SIMULATION PARAMETERS

As was described in Sec. II, v_{cut} is a parameter in the MUM algorithm and can be set optionally to different values. The larger v_{cut} is, the higher is the speed of simulation, because less muon interactions have to be simulated per unit of the muon path. But, on the other hand, a too large value of v_{cut} leads to the loss of accuracy since some essential part of fluctuations in the muon energy losses comes out of direct simulation. Thus, the question is *how large a value of* v_{cut} *may be chosen to keep the result within a desirable accuracy*? Also different models for ionization can be used; it can be optionally either treated as a completely ''continuous'' process or included in SEL. Small energy transfers strongly dominate at knock-on electron production $[d\sigma^e(E,v)/dv \propto v^{-2}]$, so this process is almost nonstochastic and it seems reasonable to exclude knock-on electrons from a simulation procedure when simulating SEL, which saves noticeable computation time. *How much does it affect the result of simulation*? Influence of these factors on a simulated result had been discussed in the literature (see, e.g. Refs. [12,22,24,25]) but in our opinion a more detailed analysis was lacking. Therefore we have undertaken our own investigation, which is reported in this section. For that we performed several sets of simulations both for propagation of monoenergetic muon beams and atmospheric muons sampled by sea level spectrum (in the later case we limited ourselves by simulation of only vertical muons) through pure water down to depths from $D=1$ km to $D=40$ km. Of course, distances of more than several kilometers for vertical muons do not concern any real detector, but simulations for large depths allow us to study general regularities that correspond, e.g., to nearly horizontal directions. Several runs were done for standard rock, as well. We tested different settings of parameters, which were as follows.

(a) v_{cut}, which changed within a range of $10^{-4}\leqslant v_{cut}\leqslant 0.2$. They inner accuracy of the MUM code becomes some-

what worse at $v_{cut} \geqslant 5 \times 10^{-2}$, especially if fluctuations in ionization are not simulated (Sec. III); therefore results for $v_{cut}=0.1$ and $v_{cut}=0.2$ are presented here only to illustrate some general qualitative regularities.

(b) Model for ionization.

(c) Parametrization for a vertical sea level atmospheric muon spectrum. Two spectra were tested, namely, one proposed in Ref. [33] (basic):

$$\frac{dN}{dE} = \frac{0.175\,E^{-2.72}}{\mathrm{cm}^2\,\mathrm{s\,sr}\;\;\mathrm{GeV}}\left(\frac{1}{1+E/103\;\;\mathrm{GeV}} + \frac{0.037}{1+E/810\;\;\mathrm{GeV}}\right), \tag{4.1}$$

and the Gaisser spectrum (Ref. [34]):

$$\frac{dN}{dE} = \frac{0.14\,E^{-2.7}}{\mathrm{cm}^2\;\;\mathrm{s\,sr}\;\;\mathrm{GeV}}\left(\frac{1}{1+E/104.6\;\;\mathrm{GeV}} + \frac{0.054}{1+E/772.7\;\;\mathrm{GeV}}\right). \tag{4.2}$$

(d) Parametrization for a total cross section for the absorption of a real photon by a nucleon at photonuclear interaction $\sigma_{\gamma N}$, which was treated both according to the Bezrukov-Bugaev parametrization proposed in Ref. [35] (basic) and the ZEUS parametrization (Ref. [36]) (see Appendix A 2 for formulas).

(e) A factor k_σ, which all muon cross sections along with the stopping power due to ionization, were multiplied by to test the influence of uncertainties in muon cross sections (and, consequently, in energy losses) on the results. We applied $k_\sigma=1.0$ as a basic value but also set $k_\sigma=0.99$ and $k_\sigma=1.01$, which corresponds to the decrease and increase of total-energy loss by 1%, respectively. Note that it is an ''optimistic'' evaluation, because the real accuracy of the existing parametrization for muon cross sections is worse (see Refs. [26,32]).

For each run we fixed the muon spectra at final and several interim depths. The differences between obtained spectra were a point of investigation.

At the first set of simulations, we propagated monoenergetic muon beams of 4 fixed initial energies $E_s=1$ TeV, 10 TeV, 100 TeV, and 10 PeV, down to slant depths $D=3.2$ km, 12 km, 23 km, and 40 km, respectively, through pure water. The value D for each initial muon energy was chosen so that the majority of muons had been stopped after propagation in the given distance. This allows us to track differences in simulated results obtained with different settings of parameters for all segments of muon beam path. In each case, the propagation of 10^6 muons was simulated. Figure 4 shows the resulting survival probabilities $p=N_D/N_s$ (where $N_s=10^6$ is initial number of muons and N_D is number of muons that have survived after propagation down to the slant depth D) vs v_{cut} for final and five interim values of D. Two curves are given on each plot for two models of ionization. Also, results for $k_\sigma=1.00\pm0.01$ and for $\sigma_{\gamma N}$ parametrization according to Ref. [36] are presented as simulated with the most accurate value $v_{cut}=10^{-4}$.

The following conclusions can be made.

(a) In most cases, except for some plots of the lower row and the left column in Fig. 4 (which corresponds to low survival probabilities and low muon initial energies, respectively) uncertainty in our knowledge of muon cross sections gives the principal effect, which essentially exceeds ones from other tested parameters.

(b) The difference between survival probabilities for the two models of ionization is less appreciable the larger the muon energy is. This is quite understandable because at muon energies $E<1$ TeV, ionization represents the greatest bulk of total energy loss, and vice versa, it becomes minor at $E>1$ TeV. Thus, the contribution that is given by ionization at higher energies, is small and, its fluctuations do not play an important role. For muons with initial energies $E \gg 1$ TeV, fluctuations in ionization become important only at the very last part of the muon path and ''are not in time'' to produce some noticeable effect.

(c) Generally, parametrizations for $\sigma_{\gamma N}$, as proposed in Refs. [35,36] do not show a noticeable difference in terms of survival probabilities, and in most cases it is within statistical error or exceeds it only slightly.

(d) The increase of v_{cut} gives the effect of both signs in survival probabilities: function $p(v_{cut})$ grows at the beginning of the muon path and falls at the last part. The same ''both-sign'' dependencies are observed for the ionization model.

(e) For $v_{cut} \leqslant 0.05$, there is almost no dependence of survival probability on v_{cut} except for the very last part of the muon path, where the survival probability becomes small. Generally, the dependence $p(v_{cut})$ is less strong the larger the initial muon energy is. The last item is illustrated complementary by Fig. 5 and Fig. 6, which show that for all initial energies, E_s simulated survival probability does not depend, in fact, on v_{cut} until 90% (for $E_s=1$ TeV) to 99.5% (for $E_s=10$ PeV) muons have been stopped.

It was shown above *what is the result* of simulations with different models of ionization and values of v_{cut}. It was a special point of interest for us to track *how and why* it influences the behavior of the survival probability. Figure 7 shows how the muon spectrum resulting from a monoenergetic muon beam with initial energy $E_s=1$ TeV, transforms when its propagation is simulated through pure water down to the slant depth of 3.2 km. Results for four settings of parameters are presented by four columns of plots. The first three columns represent spectra obtained with ionization included in SEL for $v_{cut}=10^{-4}$, 10^{-2}, and 0.2. The fourth column contains spectra simulated with entirely ''continuous'' ionization and $v_{cut}=10^{-4}$. The spectra grouped into the first column represent the most accurate tuning, both for v_{cut} and the ionization model. The first three columns demonstrate that the compactness of spectra at the same slant depth is higher the greater the value of v_{cut} is. Pay attention to the right edge of the spectra that shifts toward low energies when v_{cut} increases (it is the most noticeable for $v_{cut}=0.2$). The reason is that at any slant depth, energy of the most energetic muons in the simulated beam is determined by CEL. These muons, due to statistical fluctuations, did not undergo interactions with $v \geqslant v_{cut}$ and, consequently, lost energy only by

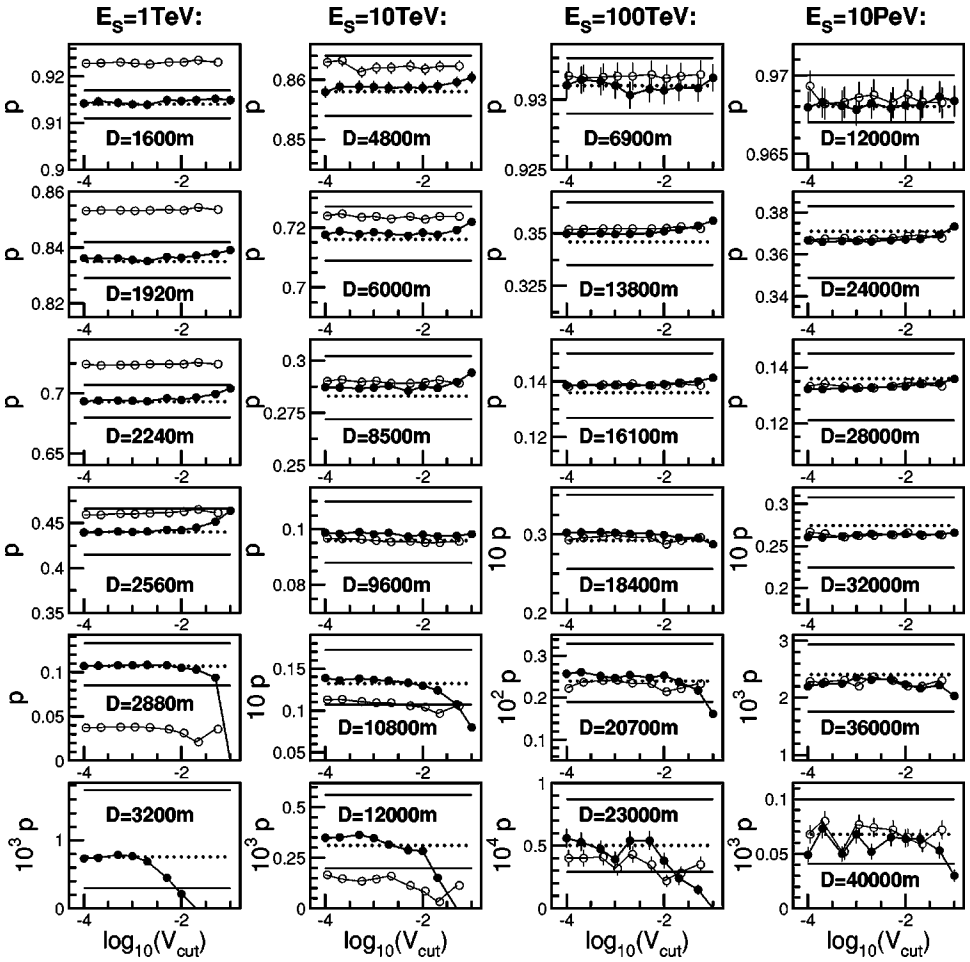

FIG. 4. Survival probabilities $p=N_D/N_s$ (where $N_s = 10^6$ is the initial number of muons in the beam and N_D is the number of muons that have survived after propagation down to slant depth D in pure water) vs v_{cut}. Values of p were obtained as a result of a simulation with MUM for monoenergetic muon beams with initial energies $E_s=1$ Tev (1st column of plots), 10 TeV (2nd column), 100 TeV (3rd column), and 10 PeV (4th column). Each column contains six plots, which correspond to six slant depths D (which differs for different E_s). Closed circles represent survival probabilities that were simulated with ionization energy losses included in SEL, open ones correspond to computation with a completely ''continuous'' model of ionization. Two horizontal solid lines on each plot show the value for survival probability computed with all muon cross sections multiplied by a factor $k_\sigma=1.01$ (lower line) and $k_\sigma=0.99$ (upper line) for $v_{cut}=10^{-4}$. Horizontal-dotted lines correspond to $v_{cut}=10^{-4}$ and the cross section for the absorption of a real photon at the photonuclear interaction is parametrized according to Ref. [36] instead of Ref. [35], which is basic in MUM. Note different scales at the Y axis.

CEL, which grows when v_{cut} increases. That is why the maximum energy in a simulated muon beam is lower for large values of v_{cut}. The fraction of muons that did not undergo a ''catastrophic'' act with $v \geqslant v_{cut}$ until given slant depth, grows with an increase of v_{cut} because the free path between two sequential interactions with $v \geqslant v_{cut}$ grows approximately as $\overline{L} \propto v_{cut}$. It leads, in particular, to distinctly visible separated picks in spectra for $v_{cut} = 0.2$, consisting just of muons which lost energy only by CEL. Also some deficit of low-energy muons appears if one sets v_{cut} to a large value. In this case the left edge of the spectrum is provided only with muons that interacted with a large fraction of lost energy while for smaller v_{cut}, an additional fraction of muons comes here. As a result, the simulated spectrum of initial monoenergetic muons at a given slant depth is more narrow if v_{cut} is large and, on the contrary, more wide if v_{cut} is small.

Now it is easy to understand how the value of v_{cut} influences simulated survival probabilities. When the simulated muon beam goes through a medium losing energy, both in CEL and SEL processes, its spectrum is constantly shifting to the left (energy decreases). For $v_{cut}=10^{-4}$, the left part of the spectrum reaches $E=0$ at a smaller slant depth compared with a larger v_{cut}, and the survival probability starts to decrease. At the same slant depth, the survival probability for $v_{cut}=10^{-2}$ and $v_{cut}=0.2$ is still equal to 1. Thus, for the first part of the path the survival probability is always larger for large v_{cut}. At some slant depth (which is equal to ~ 2.8 km in the given case) compactness of spectra simulated with large v_{cut} starts to play an opposite role. Because of more powerful CEL, muons stop faster compared with accurate simulations. So at the final part of the beam path, the simulated survival probability for large v_{cut} decreases faster compared with accurate simulation and, for instance, for v_{cut}

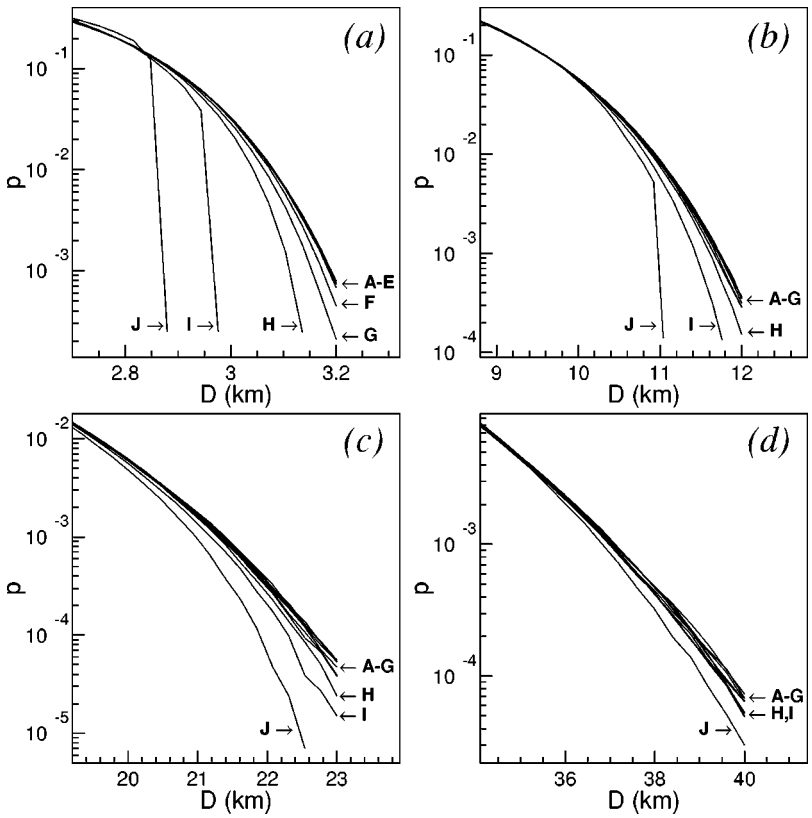

FIG. 5. The survival probability p vs slant depth D in pure water down to which the propagation of a monoenergetic muon beam with initial energy (a) $E_s=1$ TeV, (b) 10 TeV, (c) 100 TeV and (d) 10 PeV is simulated. On each plot, 10 lettered curves that correspond to different values of v_{cut}, are shown. The meaning of the letters is as follows: A: $v_{cut}=10^{-4}$, B: $v_{cut}=2\times10^{-4}$, C: $v_{cut}=5\times10^{-4}$, D: $v_{cut}=10^{-3}$, E: $v_{cut}=2\times10^{-3}$, F: $v_{cut}=5\times10^{-3}$, G: $v_{cut}=10^{-2}$, H: $v_{cut}=2\times10^{-2}$, I: $v_{cut}=5\times10^{-2}$, and J: $v_{cut}=10^{-1}$. This figure displays results that were obtained by simulation with ionization losses included in SEL. Statistical errors (which cause some unsmoothness of curves at small p) are not shown.

$=0.2$, the rest of the muon beam, which reaches the slant depth $D=2.72$ km (37% of initial number of muons) completely vanishes within the next 30 m of path, while some fraction of muons simulated with $v_{cut}=10^{-4}$ (0.07%) escapes down to the slant depth of $D=3.2$ km. Qualitatively the same effect leads to the same consequences if one treats ionization as a completely ''continuous'' process. Again, spectra become more narrow since fluctuations in ionization

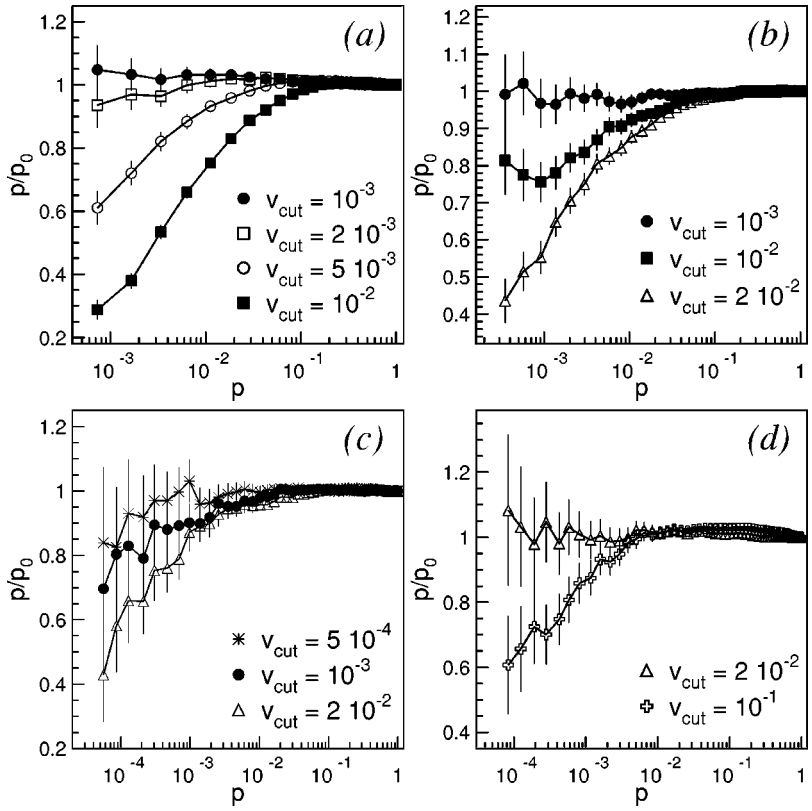

FIG. 6. The relation p/p_0 vs p. p is the survival probability for muons of initial energy (a) $E_s=1$ TeV, (b) 10 TeV, (c) 100 TeV and (d) 10 PeV at propagation through pure water with ionization included in SEL, as simulated for different values of v_{cut}; p_0 is the survival probability simulated under the same conditions for $v_{cut}=10^{-4}$. The difference in p/p_0 becomes noticeable only at $p<10^{-1}$, i.e., at the very last part of the muon beam path.

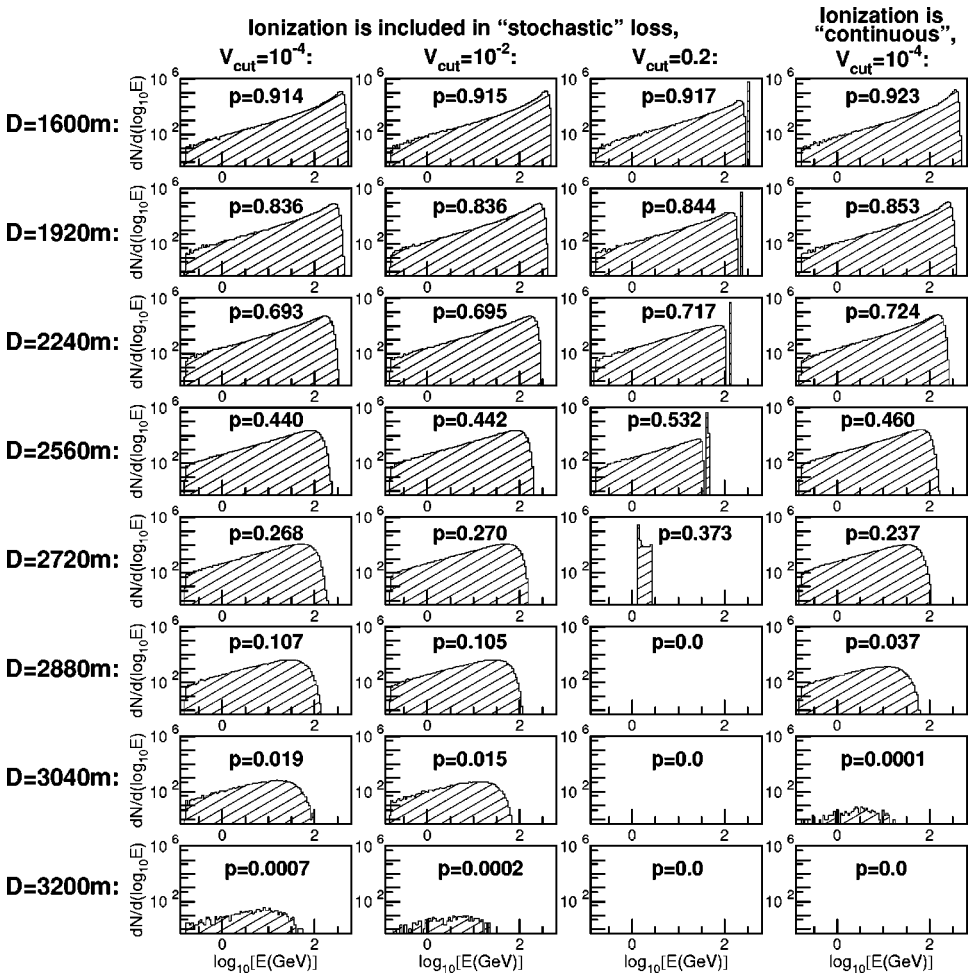

FIG. 7. The muon spectra resulting from 10^6 muons with initial energy $E_s=1$ TeV as simulated with four models for different slant depths D in pure water. The first three columns represent spectra obtained with ionization included in SEL for $v_{cut}=10^{-4}$ (first column), 10^{-2} (second column), and 0.2 (third column). The fourth column contains spectra obtained for entirely ''continuous'' ionization and $v_{cut}=10^{-4}$. On each plot, the value of the survival probability p is indicated without statistical error, which does not exceed 1%.

do not work and, as a consequence, survival probability becomes significantly higher compared with simulation with an accurate treatment of ionization at the beginning of muon beam path and falls down essentially faster at the final part of the path.

The results presented above showed the significant influence that both the model of ionization and value of v_{cut} have over the survival probability for a monoenergetic muon beam. But for practical purposes, the more important question is *how these factors work for real atmospheric muons with a power spectrum*? In Fig. 8 we present the intensity of vertical atmospheric muon flux I at different depths of pure water D from 1 km to 20 km vs v_{cut} as simulated with muons sampled according to sea level spectrum Eq. (4.1). Simulation continued until 10^4 muons reached a given depth. The curves for two models of ionization are shown for each depth along with the results for $k_\sigma=1.00\pm0.01$ at $v_{cut}=10^{-4}$, parametrization for $\sigma_{\gamma N}$ from Ref. [36] at $v_{cut}=10^{-4}$, sea level muon spectrum Eq. (4.2) at $v_{cut}=10^{-4}$, and all energy losses treated entirely as CEL (for depths $D\leqslant5$ km only). General conclusions for the case with atmospheric muons are qualitatively the same as observed for monoenergetic muon beams, but quantitatively the influence of v_{cut} and the model of ionization energy losses on the resulting muon flux at large depths is much weaker. One can reach the following conclusion:

(a) Except for the case $D=1$ km, the computed muon flux is strongly affected by accounting for fluctuations in energy losses; the muon flux intensity simulated with a nonstochastic model of energy loss is less compared with a stochastic model by 10% at 3 km w.e. and by 20% at 5 km w.e. At a depth of 20 km of pure water, the vertical muon flux computed by ignoring fluctuations, is only 10% of the simulated flux.

(b) Like the case with monoenergetic beams, 1% uncertainty in muon cross sections plays the principal role for resulting error in simulated muon depth intensity. This error has a tendency to grow with depth from $\pm2.5\%$ at a depth of 1 km w.e. to $\sim\pm15\%$ at 20 km w.e. But a particular case of this uncertainty, namely, the difference between parametrizations for $\sigma_{\gamma N}$ from Refs. [35,36], does not lead to a significant difference in the resulting intensity.

(c) The difference between muon spectra Eq. (4.1) and Eq. (4.2) leads to uncertainty from -4% ($D=1$ km) to 16% ($D=20$ km).

(d) The error that appears due to simplified, entirely ''continuous'' ionization lies, commonly, at the level of 2–3%.

(e) The dependence of simulated muon flux intensity upon v_{cut} is the most weak one compared with other studied error sources. Function $I(v_{cut})$ is almost a constant at $v_{cut}\leqslant0.05$ and changes in a range $\pm$1-2%, which is very close to statistical error. Up to $v_{cut}=0.1$, the contributed error is less

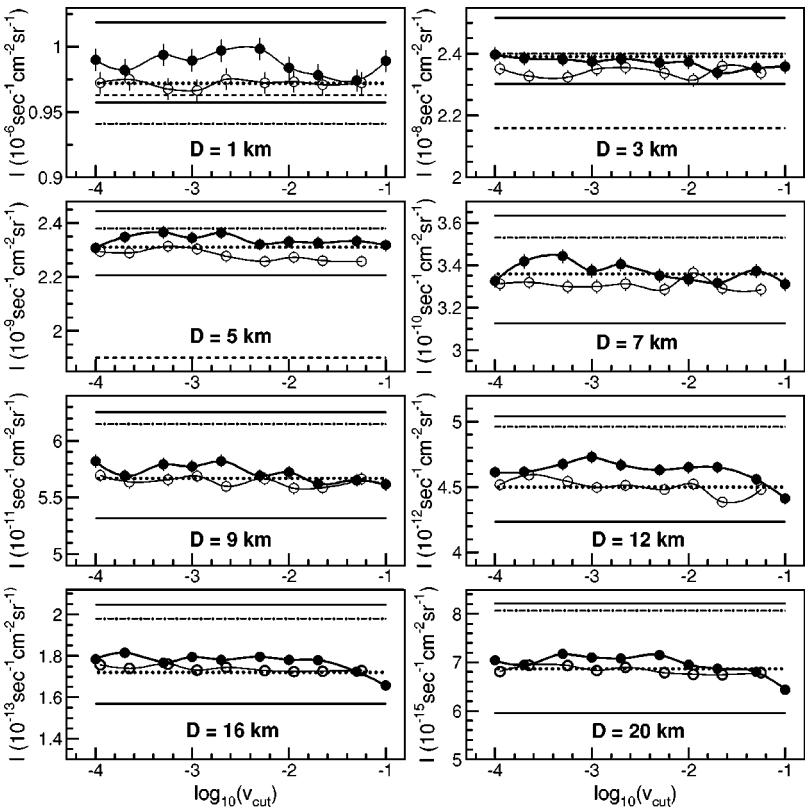

FIG. 8. The Intensity of a vertical atmospheric muon flux I at different depths D of pure water vs v_{cut} as obtained by simulation with muons sampled according to sea level spectrum from Ref. [33] [Eq. (4.1)]. Closed circles: ionization is included in SEL; and open circles: ionization is completely ''continuous.'' Two horizontal solid lines on each plot show value for survival probability simulated with all muon cross sections multiplied by a factor $k_\sigma=1.01$ (lower line) and $k_\sigma=0.99$ (upper line) for $v_{cut}=10^{-4}$. Dashed lines on plots for $D\leqslant 5$ km correspond to intensity, which was calculated for all energy losses treated as ''continuous.'' Dash-dotted lines show intensity of vertical muon flux simulated with ionization included in SEL, $v_{cut}=10^{-4}$, and muons sampled according to the Gaisser sea level spectrum [Ref. [34], Eq. (4.2)]. Horizontal-dotted lines correspond to $v_{cut}=10^{-4}$ and the cross section for absorption of a real photon at photonuclear interaction, parameterized according to Ref. [36] instead of the parametrization proposed in Ref. [35] which is basic in MUM.

than one, which comes from $\pm 1\%$ uncertainty with the muon cross sections. Also no statistically significant influence of v_{cut} upon the shape of differential atmospheric muon spectra was observed at all tested depths for $10^{-4}\leqslant v_{cut}\leqslant 0.2$ for both models of ionization energy loss.

The results reported in this section are evidence of the accuracy in parametrizations for muon cross sections and sea level spectrum to be the principal source of uncertainties when simulating atmospheric muon flux at depths where neutrino telescopes are located. It contributes uncertainty from 3% (at the depth $D=1$ km in pure water) to 15% ($D=20$ km) in the resulting intensity of muon flux. Unfortunately, this level has, at present, to be considered as a limit for the accuracy of muon propagation algorithms. The influence of the model for ionization exceeds this limit only for monoenergetic muon beams with initial energies $E\leqslant 10$ TeV and only if the level of observation is at the very last stage of the muon range where the major fraction of initial muon energy has been lost. Actually, due to the steep shape of the atmospheric muon power spectrum, an essential part of muons reaches the detector location on the last part of path. Therefore the effect also remains noticeable for real atmospheric muons, but in this case uncertainty was found to be much less, 2–3%, which is in excellent agreement with Refs. [12,24], while Ref. [25] predicts a much more significant difference (up to 17%). We suppose this disagreement may result from the fact that the ''small transfer grouping'' technique used in Ref. [25] treats muon cross sections to be constant between two interactions in contrast with the MUM algorithm. In Ref. [24] the same simplification was used but the reported results were obtained by simulation with $v_{cut}=10^{-3}$. With such a small v_{cut} the role of correct treatment for the free path is not significant (see Sec. II and Fig. 1). The choice of value for v_{cut} is even of less importance and again, it is more critical if one investigates the monoenergetic muon beam but with a power spectrum alteration in v_{cut} within $v_{cut}\leqslant 0.05$, leads only to 1%–2% differences in simulated muon flux intensities. Up to $v_{cut}=0.1$, the error caused by rough account for fluctuations in energy losses, remains less than one, which comes from uncertainties with muon energy loss. This conclusion is in a good agreement with the level of errors reported in Ref. [24]. Differences between the muon flux intensities simulated for different models of ionization and values of v_{cut}, as obtained in given work and in Refs. [24,25], are presented in Figs. 9 and 10.

So when simulating muon fluxes at large depths with an ''ideal MC muon propagation algorithm'' it is reasonable to use $v_{cut}\approx 0.05$–0.1 and an entirely ''continuous'' model for ionization. Such a setting of simulation parameters does not lead to the error that would be out of insuperable uncertainties with muon energy loss but essentially allows us to save the computation time. Figure 11 shows the dependence of computation time on v_{cut} and the model for ionization, as was obtained with the MUM algorithm. Data for muon transportation codes PROPMU (Ref. [22]) and MUSIC (Ref. [24]) are given on the figure, as well. We must emphasize that MUM in its presented version is a one-dimensional algorithm, in contrast both to PROPMU and MUSIC. PROPMU treats only Coulomb multiple scattering, while in MUSIC the angle of the muon acquired in all radiative processes is also simulated, which takes an additional computation time. We evaluate the factor by which the computation time with MUM would increase in the case of an extension up to a three-dimensional algorithm as approximately 2.

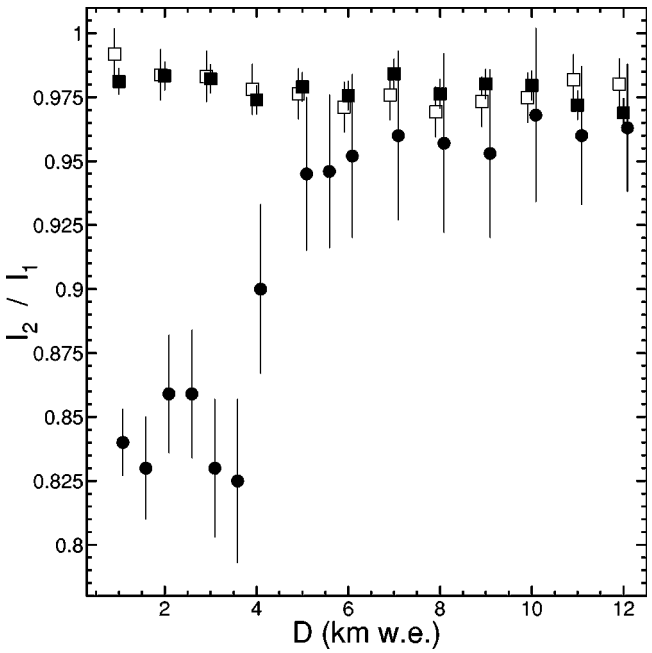

FIG. 9. Dependencies for relation I_2/I_1 vs water equivalent depth in standard rock as computed in this work (closed squares), in Ref. [24] (open squares), and in Ref. [25] (closed circles). I_1 is the depth intensity for vertical atmospheric muon flux simulated with the ionization included in SEL, I_2 the depth intensity simulated with entirely ''continuous'' ionization. Data for this work are obtained for sea level atmospheric muon spectrum from Ref. [33] [Eq. (4.1)] and $v_{cut}=10^{-3}$; data from Ref. [24] represents the result of the simulation for the sea level spectrum from Ref. [34] [Eq. (4.2)] and $v_{cut}=10^{-3}$; data from Ref. [25] were simulated with spectrum from Ref. [37] with the ''small transfer grouping'' technique.

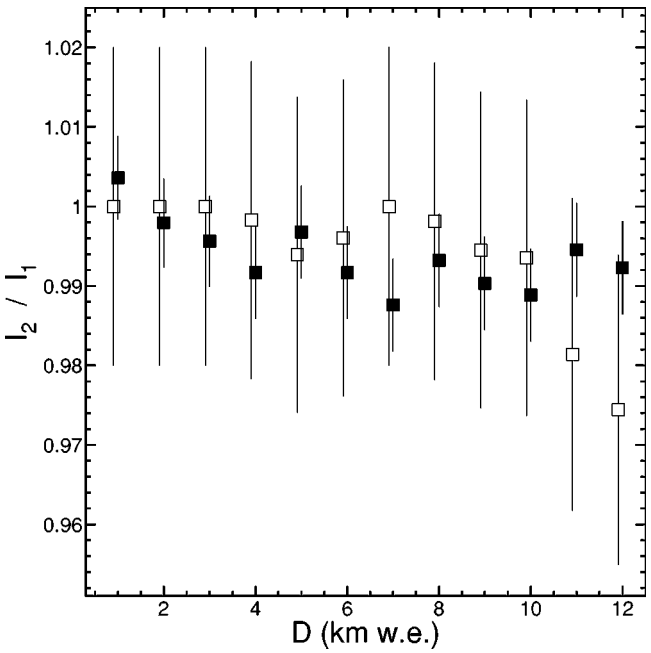

FIG. 10. The dependencies for relation I_2/I_1 vs the water equivalent depth in standard rock as computed in this work (closed squares) and in Ref. [24] (open squares). I_1 is the depth intensity for vertical atmospheric muon flux simulated with entirely ''continuous'' ionization and $v_{cut}=10^{-3}$, I_2 is the depth intensity simulated with the same treatment of ionization and $v_{cut}=10^{-2}$. Data for this work are obtained for sea level spectrum from Ref. [33] [Eq. (4.1)]; data from Ref. [24] represent the result of the simulation for the spectrum from Ref. [34] [Eq. (4.2)].

Accounting for data on the real accuracy of the current version of the MUM code (see Sec. III) and data on the computation time, as presented in Fig. 11, we conservatively consider $v_{cut}=0.05$ and the knock-on electron production included in SEL as an optimum setting for the presented algorithm, which allows us to obtain accurate results with relatively high speed. With such a setting, the proportion of computation time, which is necessary to get the same statistics with MUM, PROPMU, and MUSIC is approximately 1:10:600. Of course, for some methodical purposes, it may be necessary to choose more fine v_{cut}, e.g., if one wants to exclude an additional error when comparing results of simulations for different models of atmospheric muon sea level spectrum with each other or for investigating survival probabilities that are much more sensitive to the value of v_{cut} than the simulated spectrum of atmospheric muons at large depths.

We did not investigate the influence of simulation parameters on the results for the muon flux that originated from the neutrino, but simple argumentation may be applied for this case. In contrast with atmospheric muons whose source is far away from underwater, under-ice, or an underground detector, and whose flux may only decrease when passing from the sea level down to detector depth, the source for muons that are produced in νN interactions is uniformly distributed over water and/or rock, both outside and inside the array. The intensity of the muon flux I_μ^{ac}, which accompanies the neutrino flux in a medium, is proportional to the muon range, and, consequently, $I_\mu^{ac}\propto(dE/dx)_{total}^{-1}$, while the simulated flux of atmospheric muons at large depths depends more sharply upon muon energy loss, as was shown in this section. Thus, one may conclude that the setting of parameters described above fits even better for the propagation of muons that originated from the neutrino.

It is impossible to foresee all particular cases and give some strict conformity between the setting of parameters at the muon MC propagation code and the problem to be solved. But in this section we tried to present the whole set of data, which are necessary to choose the optimum set in each concrete case.

V. SELECTED RESULTS AND COMPARISON WITH OTHER ALGORITHMS

In this section we present selected data on survival probabilities and atmospheric muon spectra deep underwater as simulated with MUM. To obtain atmospheric muon spectra we set $v_{cut}=0.05$. As was shown in Sec. III and Sec. IV, it does not distort results compared to simulation with smaller values of v_{cut}. To compute survival probabilities, more delicate tuning was applied, $v_{cut}=10^{-3}$. In both cases ionization was included in SEL. We compare our data with data obtained with the PROPMU and MUSIC algorithms. Data simulated with

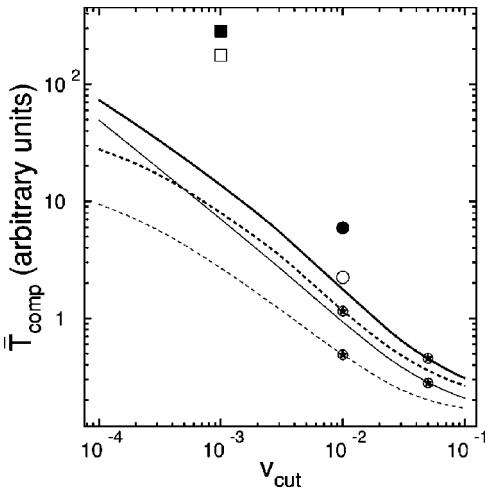

FIG. 11. The averaged computation time $\overline{T}_{comp}$, which is necessary for muon propagation in pure water vs v_{cut}, as obtained with the MUM code. The thick lines correspond to muon with initial energy $E_s=9$ TeV transported down to $D=10$ km. The thin lines are for $E_s=1$ TeV and $D=3$ km. The solid lines show the results for ionization included in SEL, and the dashed lines correspond to entirely ''continuous'' ionization. The circled asterisks on curves correspond to the conservatively evaluated upper boundary for v_{cut} below which the MUM algorithm inner accuracy has been proved to be high enough. This limit is equal to $v_{cut}=0.05$ if ionization is included in SEL and to $v_{cut}=0.01$ if ionization is entirely ''continuous'' (see Sec. III). The circles and squares show values for $\overline{T}_{comp}$, as obtained with muon propagation codes PROPMU (version 2.01, 18/03/1993 with $v_{cut}=10^{-2}$ which is unchangeable) and MUSIC (version for pure water with bremsstrahlung cross sections by Kehlner-Kokoulin-Petrukhin, 04/1999 with $v_{cut}=10^{-2}$ which is unchangeable), correspondingly. The closed markers are for $E_s=9$ TeV and $D=10$ km, and the open markers are for $E_s=1$ TeV and $D=3$ km.

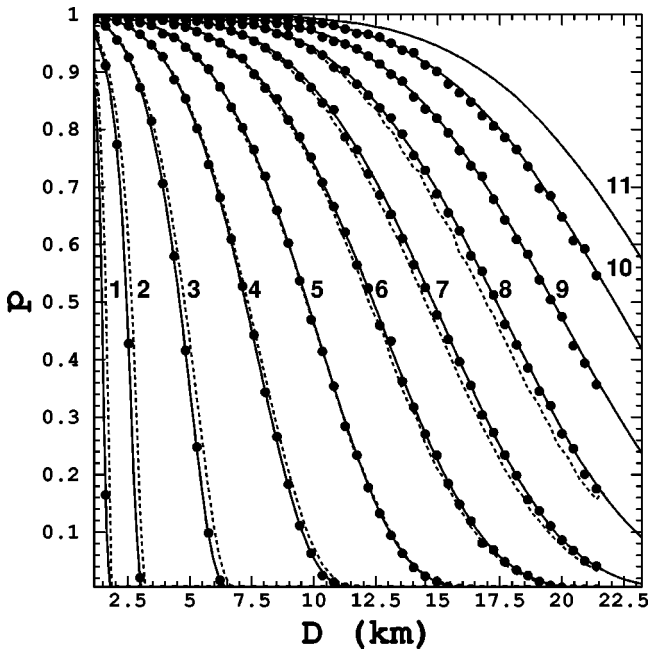

FIG. 12. The survival probabilities vs slant depth D in pure water as computed with MUM (solid lines), MUSIC (circles), and PROPMU (dashed lines). Figures near curves indicate initial energies of muon beams which were as follows: (1) 500 GeV, (2) 1 TeV, (3) 3 TeV, (4) 10 TeV, (5) 30 TeV, (6) 100 TeV, (7) 300 TeV, (8) 1 PeV, (9) 3 PeV, (10) 10 PeV, and (11) 30 PeV. At the simulations of data presented on the plot, muons are treated as stopped as soon as their energy decreases down to 10 GeV.

PROPMU [version 2.01, 18/03/1993] ($v_{cut}=10^{-2}$) and PROPMU [version 2.1, 01/2000] (both with $v_{cut}=10^{-3}$ and $v_{cut}=10^{-2}$) are very close to each other, in all figures of this section results from PROPMU [version 2.01, 18/03/1993] are presented. We used [version for pure water with bremsstrahlung cross sections by Kelner-Kokoulin-Petrukhin, 04/1999] ($v_{cut}=10^{-3}$) for MUSIC. When comparing results on atmospheric muons at large depths obtained for pure and sea water, the data are recalculated to each other using the value $\rho=1.027$ g cm^{-3} as a sea water density (Refs. [38,39]). The difference between pure and sea water is negligibly small for the muon propagation if one works in water equivalent units, which was tested by us up to a slant depth $D=10$ km w.e. (see also Ref. [13]).

Figure 12 shows survival probabilities vs slant depth D in pure water as simulated for a set of initial muon beam energies from $E_s=500$ GeV to $E_s=30$ PeV. Survival probabilities obtained with MUM coincide within statistical errors with probabilities computed with MUSIC. PROPMU gives remarkably different values which are higher compared to MUM and MUSIC output at muon energies $E_s \leqslant 30$ TeV and become less at $E_s>30$ TeV.

Figure 13 gives more detailed data on survival probabilities for three particular cases. It presents the muon spectra that resulted from monoenergetic muon beams with initial energies $E_s=1$ TeV [Fig. 13(a)], $E_s=9$ TeV [Fig. 13(b)] and $E_s=1$ PeV [Fig. 13(c)] after propagation of distances 3 km, 10 km, and 40 km in pure water, correspondingly. The distances were chosen so that survival probabilities would be much less than 1, in which case differences become more noticeable (see Sec. IV). A good agreement is observed between MUM and MUSIC data, while data obtained with PROPMU indicate essential differences that are of the same signs as in Fig. 12.

In Fig. 14, differential spectra for vertical atmospheric muons at different depths in pure water are presented as simulated with MUM, PROPMU, and MUSIC. Muons at the surface were sampled according to the spectrum Eq. (4.1). Also parametrizations for deep underwater muon spectra as proposed by Okada [40] and by Klimushin, Bugaev and Sokalski (KBS) [33] are shown. The KBS parametrization can adopt different models for sea level atmospheric muon spectrum. For data presented in Fig. 14, we used the spectrum Eq. (4.1), which is a basic one for the KBS parametrization. MUM gives almost the same results as MUSIC, which should be expected because the survival probabilities for muons in pure water are the same when simulating with MUSIC and MUM, as was shown above. Simulation with PROPMU produces the muon spectra which (a) are significantly higher (31%, 30%, 27%, and 17% in terms of integral muon flux at the depths $D=1$ km, 3 km, 6 km, and 10 km, respectively) and (b) are expanded to the low energies. It is in good quali-

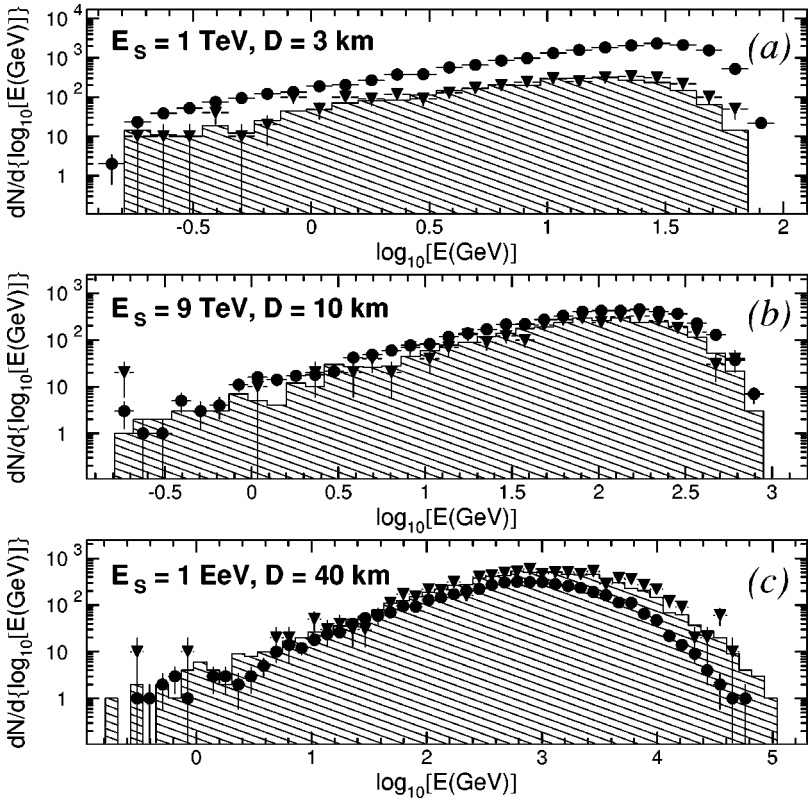

FIG. 13. The Muon spectra resulting from monoenergetic muon beams with initial energies (a) $E_s=1$ TeV, (b) $E_s=9$ TeV, and (c) $E_s=1$ EeV (c) after propagation down to depths $D=3$ km, 10 km, and 40 km of pure water, correspondingly, as simulated with MUM (histograms), PROPMU (circles), and MUSIC (triangles). The corresponding values for survival probabilities p (fraction of muons survived after propagation) are equal to $p(1\ \text{TeV}, 3\ \text{km}) = 0.029$ (MUM), 0.033 (MUSIC), 0.19 (PROPMU); $p(9\ \text{TeV}, 10\ \text{km}) = 0.030$ (MUM), 0.031 (MUSIC), 0.048 (PROPMU); $p(1\ \text{PeV}, 40\ \text{km}) = 0.078$ (MUM), 0.084 (MUSIC), and 0.044 (PROPMU).

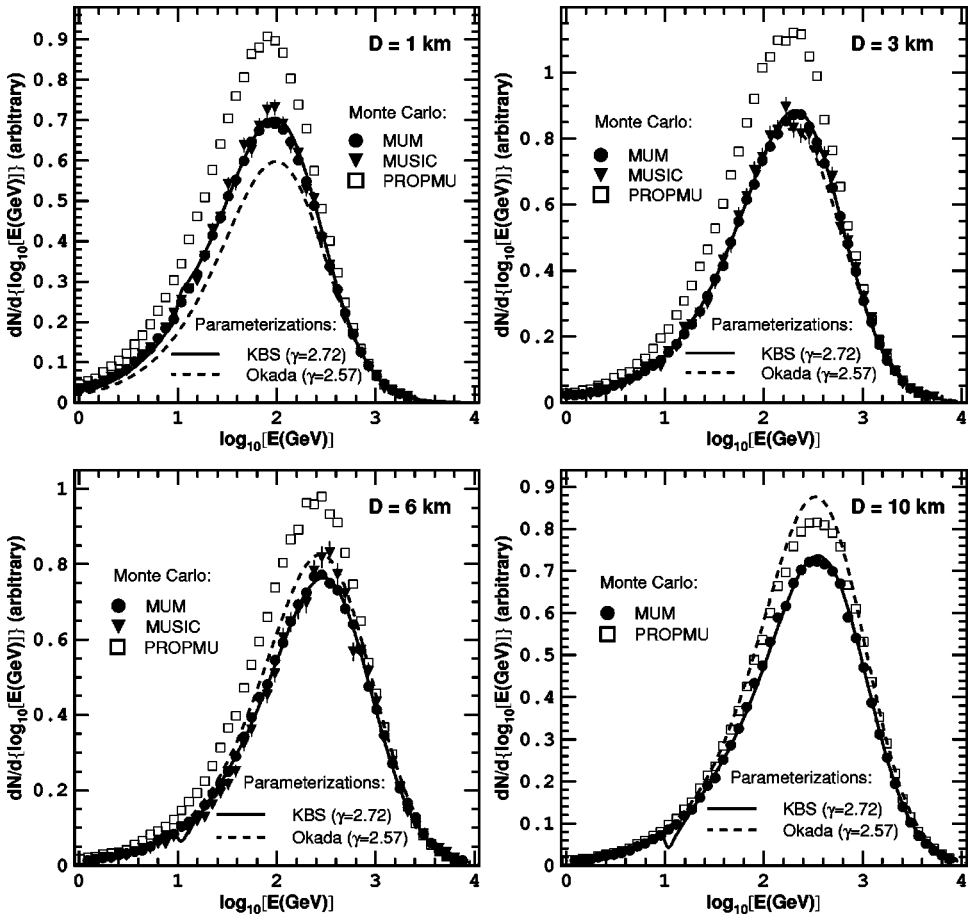

FIG. 14. The differential spectra of vertical atmospheric muons at four depths in the pure water as simulated with MUM, PROPMU, and MUSIC [in all cases muon energies at the sea level were sampled according to spectrum Eq. (4.1)] and parameterized according to KBS with sea level spectrum Eq. (4.1) (Ref. [33]) and Okada (Ref. [40]).

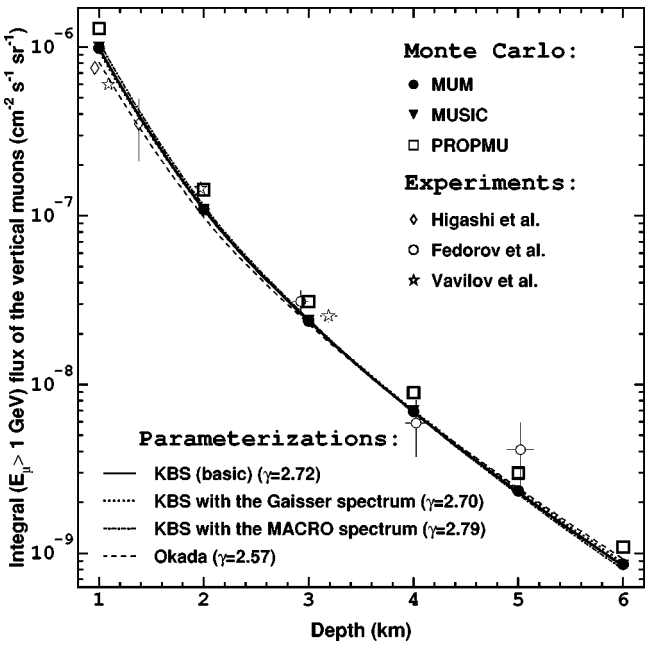

FIG. 15. Results for the integral flux of vertical atmospheric muons vs depth in pure water as (1) simulated with MUM, PROPMU, and MUSIC with sea level spectrum Eq. (4.1); (2) parameterized by KBS (Ref. [33]) with sea level atmospheric muon spectra Eq. (4.1) (basic), from Ref. [34] (the Gaisser spectrum), from Ref. [42] (the MACRO spectrum), and Okada (Ref. [40]) with sea level spectrum from Ref. [41]; (3) measured by Higashi *et al.* (Ref. [38]), Fedorov *et al.* (Ref. [43]), and Vavilov *et al.* (Ref. [44]).

tative agreement with the results on survival probabilities presented in Figs. 12 and 13. The coincidence between spectra simulated with MUM and the curves for the basic KBS parametrization results from the fact that in both cases the same sea level atmospheric muon spectrum was adopted and, besides, muon transport with the MUM algorithm was applied to obtain the KBS parametrization. We would like to mark that the survival probabilities that KBS parametrization is based on, were computed with $v_{cut}=10^{-3}$. An excellent agreement with direct simulation in which $v_{cut}=0.05$ was set, confirms the conclusion concerning insensitivity of the results on simulated atmospheric muon spectra at large depths on a value of v_{cut} up to at least $v_{cut}=0.05$ (see Sec. IV). The Okada parametrization is lower than KBS, MUM, and MUSIC results (up to 18% in terms of the integral muon flux at $D=1$ km) at relatively shallow depths, and becomes higher at $D\geqslant 5$ km because it is based on a rather hard sea level atmospheric muon spectrum with an index $\gamma=2.57$ (Ref. [41]) which leads to a deficit for low-energy muons compared to the basic KBS parametrization.

Figure 15 presents the results on the integral flux of vertical atmospheric muons at large depths in pure water as (a) simulated with MUM, PROPMU, and MUSIC for sea level spectrum Eq. (4.1); (b) parameterized by KBS (Ref. [33]) with sea level atmospheric muon spectra Eq. (4.1) (basic), from Ref. [34] (the Gaisser spectrum), from Ref. [42] (the MACRO spectrum) and Okada (Ref. [40]) with sea level spectrum from Ref. [41]; (c) measured by Higashi *et al.* (Ref. [38]), Fedorov *et al.* (Ref. [43]) and Vavilov *et al.* (Ref. [44]). Note that ''experimental'' points on the plot do not represent the pure experimental data because authors had to recalculate obtained counting rates to the vertical direction using a model for the muon angular spectrum underwater. MUM and MUSIC results coincide with each other within 1–2%. Results from the PROPMU algorithm exceed points from MUSIC and MUM by ~30%, higher than any of the presented parametrizations.

We also compared the data on muon propagation through the standard rock obtained with MUM and MUSIC. The mean energy for vertically down-going atmospheric muons sampled with the sea level spectrum from Ref. [34] was computed with MUM as $\bar{E}=123\pm 2$ GeV, 256 ± 4 GeV, and 387 ± 7 GeV at depths $D=1$ km w.e., 3 km w.e., and 10 km w.e., respectively. The corresponding values simulated with the MUSIC code and reported in Ref. [24] are $\bar{E}=125\pm 1$ GeV, 259 ± 3 GeV, and 364 ± 4 GeV. So the maximum difference observed at the depth $D=10$ km w.e. is 6%.

Thus, results on survival probabilities and atmospheric muon spectra at large depths as simulated with MUM, are practically in a coincidence with results obtained with MUSIC and are also not in contradiction with any experimental and theoretical results presented in this section. The PROPMU algorithm shows noticeable differences with MUM, which are in good qualitative agreement to each other; higher survival probabilities lead to higher muon fluxes deep underwater. It is difficult to clarify the source of observed discrepancies without a detailed comparison for all steps of the algorithms, but we believe that they cannot be explained only by a difference in models for muon energy loss, as is used in MUM (see Appendix A) and PROPMU (Refs. [19,22]) which does not exceed 2% at $E\leqslant 10$ TeV (in terms of stopping power) besides being of both signs.

More data obtained with the MUM algorithm can be found in Ref. [33].

VI. CONCLUSIONS

We have presented the muon propagation Monte Carlo FORTRAN code MUM and have given selected results obtained with the code for muon spectra at large depths and survival probabilities in comparison with results obtained with other muon transportation algorithms. It was shown that for a majority of applications, it is quite enough to account only for fluctuations in the radiative energy loss with fractions of energy lost as large as $v\geqslant v_{cut}=0.05$–0.1, while ionization energy loss may be entirely accounted for by the stopping power formula, as well as radiative energy loss with fractions of energy lost $v<v_{cut}=0.05$–0.1. This gives an essential advantage in terms of the computation time compared to commonly used $v_{cut}=10^{-3}$–10^{-2} without loss of accuracy when simulating both propagation of atmospheric muons, and muons that are born in νN interactions. However, in practice, it makes particular demands to the accuracy of the MC algorithm. Some customary simplifications [e.g., Eq. (2.4)] which work perfectly when $v_{cut}=10^{-3}$–10^{-2} become sources of significant errors when v_{cut} increases. The sign and value of these errors depend also on whether fluctuations

in ionization are accounted for or not. So for the presented version of the MUM algorithm, the optimum set of simulation parameters was conservatively evaluated by us (accounting results on inner accuracy test and dependence of computation time on v_{cut}) to be $v_{cut}=0.05$ with a knock-electron production included in SEL.

Our viewpoint on the advantages of MUM is as follows. It is flexible enough and provides, with eventuality, the ability to tune parameters of simulation to an optimum for each concrete case in order to get desirable equilibrium between computation time and accuracy. Medium composition and parametrizations for the muon cross sections are easily changeable. The inner accuracy of the code was conservatively evaluated to be 2×10^{-3} or better. Besides, MUM provides the special routine that allows to test the inner accuracy for each given set of simulation parameters and take it into account when evaluating the significance of the results. The main disadvantage is that MUM, in its reported version, still does not treat the three dimensions as do, e.g., PROPMU and MUSIC codes. So it cannot be used to obtain lateral and angular deviations of muons at propagation through matter. Also other important features are still missing in MUM—for instance, the treatment of the composed medium as is possible, e.g., in the latest version of the MUSIC code (Ref. [45]). But we consider the current version of MUM[1] as a basis for further development and plan to complement it, step-by-step, for all necessary features.

ACKNOWLEDGMENTS

We would like to express our gratitude to I. Belolaptikov for useful discussions which allowed us to improve the MUM algorithm. We are grateful to A. Butkevich, R. Kokoulin, V. Kudryavzev, P. Lipari, W. Lohmann, V. Naumov, O. Streicher, and Ch. Wiebusch who read the paper at the draft stage and gave their comments, which mostly were taken into account both in the final version of the article and in the algorithm itself. One of us (I.S.) has benefited a lot by the support of L. Bezrukov and Ch. Spiering.

APPENDIX A: PARAMETRIZATIONS FOR MUON CROSS SECTIONS USED IN THE MUM ALGORITHM

We use the following designations in this section: $\alpha=7.297353\times10^{-3}$—fine structure constant; $r_e=2.817941\times10^{-13}$ cm—classical radii of electron; $m_\mu=0.1056593$ GeV and $m_e=0.5110034$ MeV—muon and electron masses, respectively; $N_A=6.022\times10^{23}$—the Avogadro number; Z and A—electric charge and atomic weight, respectively; $e=2.718282$; $\pi=3.141593$. Other notations are explained in comments to formulas when necessary.

1. Bremsstrahlung

We use the differential cross section for bremsstrahlung as parametrized by Andreev, Bezrukov, and Bugaev in Ref. [46] as a basic parametrization:

$$\frac{d\sigma^b}{dv}(E,v)=\alpha\left(2r_eZ\frac{m_e}{m_\mu}\right)^2\frac{1}{v}\left[(2-2v+v^2)\Psi_1(q_{\min},Z)-\frac{2}{3}(1-v)\Psi_2(q_{\min},Z)\right],$$

$$\Psi_{1,2}(q_{\min},Z)=\Psi^0_{1,2}(q_{\min},Z)-\Delta_{1,2}(q_{\min},Z),$$

$$\Psi^0_1(q_{\min},Z)=\frac{1}{2}\left(1+\ln\frac{m_\mu^2a_1^2}{1+x_1^2}\right)-x_1\arctan\frac{1}{x_1}+\frac{1}{Z}\left[\frac{1}{2}\left(1+\ln\frac{m_\mu^2a_2^2}{1+x_2^2}\right)-x_2\arctan\frac{1}{x_2}\right],$$

$$\Psi^0_2(q_{\min},Z)=\frac{1}{2}\left(\frac{2}{3}+\ln\frac{m_\mu^2a_1^2}{1+x_1^2}\right)+2x_1^2\left(1-x_1\arctan\frac{1}{x_1}+\frac{3}{4}\ln\frac{x_1^2}{1+x_1^2}\right)$$
$$+\frac{1}{Z}\left[\frac{1}{2}\left(\frac{2}{3}+\ln\frac{m_\mu^2a_2^2}{1+x_2^2}\right)+2x_2^2\left(1-x_2\arctan\frac{1}{x_2}+\frac{3}{4}\ln\frac{x_2^2}{1+x_2^2}\right)\right],$$

$$\Delta_1(q_{\min},Z\neq1)=\ln\frac{m_\mu}{q_c}+\frac{\zeta}{2}\ln\frac{\zeta+1}{\zeta-1},\quad \Delta_2(q_{\min},Z\neq1)=\ln\frac{m_\mu}{q_c}+\frac{\zeta}{4}(3-\zeta^2)\ln\frac{\zeta+1}{\zeta-1}+\frac{2m_\mu^2}{q_c^2},$$

$$\Delta_{1,2}(q_{\min},Z=1)=0,\quad q_{\min}=\frac{m_\mu^2v}{2E(1-v)},\quad x_i=a_iq_{\min},\quad a_1=\frac{111.7}{Z^{1/3}m_e},\quad a_2=\frac{724.2}{Z^{2/3}m_e},\quad \zeta=\sqrt{1+\frac{4m_\mu^2}{q_c^2}},\quad q_c=\frac{1.9m_\mu}{Z^{1/3}}.$$

The integration limits for bremsstrahlung in Eqs. (2.1), (2.3), (2.6), and (3.3) are

[1]The MUM code is available on request to sokalski@pcbai10.inr.ruhep.ru

$$v^b_{min}=0, \quad v^b_{max}=1-\frac{3}{4}\sqrt{e}\,(m_\mu/E)Z^{1/3}.$$

Note that this parametrization does not account for the contribution from e diagrams for bremsstrahlung when γ quantum is emitted by atomic electrons, which are knocked on by recoil (Ref. [47]). Corresponding corrections are done in parametrizations for knock-on electron production (see Appendix A 4) according to Ref. [48]. Optionally, the differential cross section for muon bremsstrahlung can be also treated in MUM according to the parametrization given by Kelner, Kokoulin, and Petrukhin (Refs. [47,48]).

2. Photonuclear interaction

We use parametrization for the photonuclear interaction of muon proposed by Bezrukov and Bugaev (Ref. [35]):

$$\frac{d\sigma^n}{dv}=\frac{\alpha}{8\pi}A\sigma_{\gamma N}v\left\{H(v)\ln\left(1+\frac{m_2^2}{t}\right)-\frac{2m_\mu^2}{t}\left[1-\frac{0.25m_2^2}{t}\ln\left(1+\frac{t}{m_2^2}\right)\right]+G(z)\left\{H(v)\left[\ln\left(1+\frac{m_1^2}{t}\right)-\frac{m_1^2}{m_1^2+t}\right]-\frac{2m_\mu^2}{t}\left(1-\frac{0.25m_1^2}{m_1^2+t}\right)\right\}\right\},$$

$$H(v)=1-\frac{2}{v}+\frac{2}{v^2},$$

$$G(z)=\frac{9}{z}\left[\frac{1}{2}+\frac{(1+z)e^{-z}-1}{z^2}\right] \qquad (Z\neq 1),$$

$$G(z)=3 \qquad (Z=1),$$

$$z=0.00282A^{1/3}\sigma_{\gamma N}, \quad t=\frac{m_\mu^2 v^2}{1-v},$$

$$m_1^2=0.54\ \text{GeV}^2, \quad m_2^2=1.80\ \text{GeV}^2.$$

The total cross section for the absorption of a real photon of energy $\nu=s/2m_N=vE$ by a nucleon, $\sigma_{\gamma N}$, can be calculated in MUM optionally, according to either the parametrization from Ref [35] (basic):

$$\sigma_{\gamma N}=[114.3+1.647\ln^2(0.0213\,\nu)]\,\mu b,$$

or by the ZEUS parametrization (Ref. [36]):

$$\sigma_{\gamma N}=(63.5\,s^{0.097}+145\,s^{-0.5})\,\mu b,$$

where s and ν are expressed in GeV^2 and GeV, respectively.

The parametrization (Ref. [35]) is valid for $\nu>1$ GeV, so we use values $v^n_{min}=0.8/E(\text{GeV})$ and $v^n_{max}=1$ as integration limits in Eqs. (2.1), (2.3), (2.6), and (3.3). Note that the results of the integration were tested to be almost insensitive to the lower limit in a wide range $0.2/E(\text{GeV}) \leqslant v^n_{min} \leqslant 1.5/E(\text{GeV})$.

3. Direct electron-positron pair production

The cross section for direct e^+e^--pair production is used in MUM as parametrized by Kokoulin and Petrukhin (Refs. [48,49]):

$$\frac{d\sigma^p}{dv}(E,v)=\alpha^2\frac{2}{3\pi}r_e^2Z[Z+\zeta(Z)]\frac{1-v}{v}\times\int_\rho[\Phi_e+(m_e/m_\mu)^2\Phi_\mu]d\rho,$$

$$\Phi_e=\left\{[(2+\rho^2)(1+\beta)+\xi(3+\rho^2)]\ln\left(1+\frac{1}{\xi}\right)+\frac{1-\rho^2-\beta}{1+\xi}-(3+\rho^2)\right\}L_e,$$

$$\Phi_\mu=\left\{\left[(1+\rho^2)\left(1+\frac{3}{2}\beta\right)-\frac{1}{\xi}(1-\rho^2)(1+2\beta)\right]\ln(1+\xi)+\frac{\xi(1-\rho^2-\beta)}{1+\xi}+(1-\rho^2)(1+2\beta)\right\}L_\mu,$$

$$L_e=\ln\left[\frac{R\,Z^{-1/3}\sqrt{(1+\xi)(1+Y_e)}}{1+[2m_e\sqrt{e}R\,Z^{-1/3}(1+\xi)(1+Y_e)]/E\,v(1-\rho^2)}\right]-\frac{1}{2}\ln\left[1+\left(\frac{3}{2}\frac{m_e}{m_\mu}Z^{1/3}\right)^2(1+\xi)(1+Y_e)\right],$$

$$L_\mu=\ln\left[\frac{\frac{2}{3}\frac{m_\mu}{m_e}R\,Z^{-2/3}}{1+[2m_e\sqrt{e}R\,Z^{-1/3}(1+\xi)(1+Y_e)]/E\,v(1-\rho^2)}\right],$$

$$Y_e=\frac{5-\rho^2+4\beta(1+\rho^2)}{2(1+3\beta)\ln(3+1/\xi)-\rho^2-2\beta(2-\rho^2)},$$

$$Y_\mu=\frac{4+\rho^2+3\beta(1+\rho^2)}{(1+\rho^2)\left(\frac{3}{2}+2\beta\right)\ln(3+\xi)+1-\frac{3}{2}\rho^2},$$

$$\beta=\frac{v^2}{2(1-v)}, \quad \xi=\left(\frac{m_\mu v}{2m_e}\right)^2\frac{(1-\rho^2)}{(1-v)}.$$

Here $\rho=(\epsilon^+-\epsilon^-)/(\epsilon^++\epsilon^-)$ is the asymmetry coefficient of the energy distribution of the e^+e^- pair, where ϵ^+ and ϵ^- are positron and electron energies, respectively. The limits for integration over ρ are determined by

$$0\leqslant|\rho|\leqslant\left(1-\frac{6m_\mu^2}{E^2(1-v)}\right)\sqrt{1-\frac{4m_e}{Ev}}.$$

R is a parameter determined by the value of radiation logarithm ($R=183$ for the Thomas-Fermi model and slightly depends upon Z for the Hartree-Fock model). Its values are taken from Ref. [50], where R has been calculated for different atoms according to the Hartree-Fock model. $\zeta(Z)\approx 1$ takes into account the pair production in collisions with electrons. The values from $\zeta(Z)$ are computed according to Refs. [48,51]. The integration limits for $j=p$ in Eqs. (2.1), (2.3), (2.6), and (3.3) are

$$v^p_{min}=\frac{4m_e}{E},\quad v^p_{max}=1-\frac{3}{4}\sqrt{e}\,(m_\mu/E)Z^{1/3}.$$

4. Knock-on electron production

The cross section for knock-on electron production is parametrized in the MUM algorithm as follows:

$$\frac{d\sigma^e}{dv}(E,v)=2\pi r_e^2 Z\frac{m_e}{E}\left(\frac{1}{v^2}-\frac{1}{v}\frac{E}{v^e_{max}}+\frac{1}{2}\right)[1+\Delta_{e\gamma}(E,v)],$$

$$v^e_{max}=\frac{2m_eE}{m_\mu^2+2m_eE}.$$

$\Delta_{e\gamma}(E,v)$ represents the correction that takes into account e diagrams for bremsstrahlung (Refs. [47,48]) resulting in the additional recoil of electrons:

$$\Delta_{e\gamma}(E,v)=\frac{\alpha}{2\pi}\ln\left(1+\frac{2vE}{m_e}\right)\left[\ln\left(\frac{4E^2(1-v)}{m_\mu^2}\right)-\ln\left(1+\frac{2vE}{m_e}\right)\right],$$

The value of v^e_{max} is also used as an upper integration limit in Eqs. (2.3) and (2.6) for $j=e$.

5. Ionization

Following Refs. [47,48], in the MUM code we treat the e diagrams for bremsstrahlung as a part of the ionization process. Therefore we have to use a bit modified formula for ionization:

$$\left[\frac{dE}{dx}(E)\right]_{ion}=\frac{K}{\beta^2}\frac{Z}{A}\rho\left[\ln\left(\frac{2m_ep^2E_{\max}}{m_\mu^2\overline{I^2}}\right)+\frac{E^2_{\max}}{4E^2}-2\beta^2-\delta\right]+\frac{N_A}{A_{eff}}\rho E\sum_{i=1}^{n}\left[k_i\int_0^{v^e_{max}}\Delta_{e\gamma}(E,v)v\,dv\right].$$

Here $K=0.1535$ MeV g^{-1} cm^2, p is the muon momentum, $\beta=p/E$ is the muon velocity, ρ is the material density, $\overline{I}$ is the mean ionization potential,

$$E_{\max}=(2m_ep^2)/(m_\mu^2+m_e^2+2m_eE)$$

is the maximum energy transferable to an electron, δ is the density-effect correction, which is treated according to Ref. [52]:

$$\delta=\theta(X-X_0)[4.6052X+a\,\theta(X_1-X)(X_1-X)^m+C],$$

where θ is the step function [$\theta(x)=0$ at $x\leqslant 0$ and $\theta(x)=1$ at $x>0$], and $X=\log_{10}(p/m_\mu)$. The values X_0,X_1,a,m, and C depend on the material and can be found in Refs. [19,52] along with the values for $\overline{I}$, ρ, and Z/A. The first term represents the Bethe-Bloch formula with corrections for the density effect, the second one accounts for bremsstrahlung e diagrams. Expressions for $\Delta_{e\gamma}(E,v)$ and v^e_{max} are given in Appendix A 4, and the meaning of the values A_{eff} and k_i is explained in Sec. II.

APPENDIX B: FREE PATH BETWEEN TWO MUON INTERACTIONS

For the proof of the set of equation Eqs. (2.2) it is convenient to introduce the kinetic equation for a propagation of a monoenergetic muon beam through a medium. With the notations used in textbooks, this equation has the following view:

$$\partial n(E,t)/\partial t-\partial[\beta(E)n(E,t)]/\partial E+n(E,t)/\lambda(E)=0,$$
$$n(E,0)=n_0\delta(E-E_0). \tag{B1}$$

Here, $n(E,t)$ is the number of muons with energy E after propagation of distance t, $\beta(E)$ is the "continuous" energy loss per unit path, and $\lambda(E)$ is the muon mean free path before the interaction of the SEL type. The solution of Eq. (B1) is

$$n(E,t)=n_0\delta[E-\epsilon(E_0,t)]\exp\left[-\int_E^{E_0}dE'/[\lambda(E')\beta(E')]\right], \tag{B2}$$

where $\epsilon(E_0,t)$ is found from the equation

$$\int_{\epsilon(E_0,t)}^{E_0}dE/\beta(E)=t. \tag{B3}$$

Notice that Eq. (B2) can be rewritten as

$$\eta(E,t)=\delta[E-\epsilon(E_0,t)]\exp\left[-\int_E^{E_0}dE'/[\lambda(E')\beta(E')]\right], \tag{B4}$$

where $\eta(E,t)$ is the probability for a single muon to pass the path t without the interaction of the SEL type, and then one can easily see that Eqs. (B3) and (B4) lead to the Eqs. (2.2) after the following substitutions, which are necessary for a return to the notations of Sec. II:

$$E_0\to E_1,\quad E\to E_2,\quad \lambda(E)\to\overline{L}(E),$$
$$\beta(E)\to[dE(E)/dx]_{CEL},\quad t\to L.$$

[1] G.T. Zatsepin and E.D. Mikhalchi, J. Phys. Soc. Jpn. **17**, 356 (1962).
[2] K. Kobayakawa, Nuovo Cimento Soc. Ital. Fis., B **47**, 156 (1967).
[3] S. Hayakawa, *Cosmic Ray Physics–Nuclear and Astrophysical Aspects*, Interscience Monographs and Texts in Physics and Astronomy Vol. XXII, edited by R. E. Marshak (University of Rochester, New York, 1969).
[4] E. Kiraly, P. Kiraly, and J.L. Osborn, J. Phys. A **5**, 444 (1972).
[5] A. Misaki and J. Nishimura, Uchusen Kenkyu **21**, 250 (1976).
[6] V.I. Gurentsov, G.T. Zatsepin, and E.D. Mikhalchi, Yad. Fiz. **23**, 1001 (1976) [Sov. J. Nucl. Phys. **23**, 527 (1976)].
[7] Y. Minorikawa, T. Kitamura, and K. Kobayakawa, Nuovo Cimento Soc. Ital. Fis., C **4**, 471 (1981).
[8] E.V. Bugaev, V.A. Naumov, and S.I. Sinegovsky, Yad. Fiz. **41**, 383 (1985) [Sov. J. Nucl. Phys. **41**, 245 (1985)]; Izv. Akad. Nauk SSSR, Ser. Fiz. **49**, 1389 (1985) [Proc. of the Acad. of Sci. of the USSR, Phys. Ser. **49**, 146 (1985)].
[9] D.P. Bhattacharyya, Nuovo Cimento Soc. Ital. Fis., C **9**, 404 (1986).
[10] O.C. Allkofer and D.P. Bhattacharyya, Phys. Rev. D **34**, 1368 (1986).
[11] V.N. Bakatanov *et al.*, Yad. Fiz. **55**, 2107 (1992) [Sov. J. Nucl. Phys. **55**, 1169 (1992)].
[12] V.A. Naumov, S.I. Sinegovsky, and E.V. Bugaev, Yad. Fiz. **57**, 439 (1994) [Phys. At. Nucl. **57**, 412 (1994)].
[13] E.V. Bugaev *et al.*, Phys. Rev. D **58**, 054001 (1998).
[14] P.J. Hayman, N.S. Palmer, and A.W. Wolfendale, Proc. R. Soc. London **A275**, 391 (1963).
[15] J.L. Osborn, A.W. Wolfendale, and E.C.M. Young, J. Phys. A **1**, 55 (1968).
[16] L. Bergamasco and P. Picchi, Nuovo Cimento Soc. Ital. Fis., B **3**, 134 (1971).
[17] Yu.N. Vavilov, Yu.A. Trubkin, and V.M. Fedorov, Yad. Fiz. **18**, 884 (1974) [Sov. J. Nucl. Phys. **18**, 434 (1974)].
[18] N. Takahashi *et al.*, Uchusen Kenkyu **28**, 120 (1984).
[19] W. Lohmann, R. Kopp, and R.Voss, CERN Report No. 85-03, 1985.
[20] J.N. Capdevielle *et al.*, J. Phys. G **11**, 565 (1985).
[21] H. Bilokon *et al.*, Nucl. Instrum. Methods Phys. Res. A **303**, 381 (1991).
[22] P. Lipari and T. Stanev, Phys. Rev. D **44**, 3543 (1991).
[23] K. Mitsui, Phys. Rev. D **45**, 3051 (1992).
[24] P. Antonioli *et al.*, Astropart. Phys. **7**, 357 (1997); V.A. Kudryavtsev *et al.*, Phys. Lett. B **471**, 251 (1999).
[25] A.A. Lagutin, P.B. Togobitsky, and A. Misaki, Izv. Altayskogo Gos. Universiteta special issue, 93 (1998).
[26] W. Rhode and C. Cârloganu, in *Proceedings of the Workshop on Simulation and Analysis Methods for Large Neutrino Telescopes*, Zeuthen, 1998, edited by C. Spiering (DESY Zeuthen, Zeuthen, 1998), p. 247.
[27] Baikal Collaboration Report No. 92/11, edited by Ch. Spiering and I. Sokalski, 1992; Baikal Collaboration, V.A. Balkanov *et al.*, Nucl. Phys. B (Proc. Suppl.) **87**, 405 (2000).
[28] S. Barwick *et al.*, Wisconsin University Report No. MAD-PH-629, 1991; E. Andres *et al.*, Astropart. Phys. **13**, 1 (2000).
[29] E. Aslanides *et al.*, astro-ph/9907432; P. Amram *et al.*, Nucl. Phys. B (Proc. Suppl.) **75A**, 415 (1999).
[30] L.K. Resvanis *et al.*, Nucl. Phys. B (Proc. Suppl.) **35**, 294 (1994); S. Bottai *et al.*, *ibid.* **85**, 153 (2000).
[31] E.V. Bugaev, I.A. Sokalski, and S.I. Klimushin, hep-ph/0010323.
[32] R. P. Kokoulin and A. A. Petrukhin, in *Proceedings of the 22nd International Cosmic Ray Conference*, Dublin, 1991, edited by M. Cawley *et al.* (The Dublin Institute for Advanced Studies, Dublin, 1991), Vol. 4, p. 536; R.P. Kokoulin, Nucl. Phys. B (Proc. Suppl.) **70**, 475 (1999).
[33] S.I. Klimushin, E.V. Bugaev, and I.A. Sokalski, Phys. Rev. D **64**, 014016 (2001).
[34] T. K. Gaisser, *Cosmic Rays and Particle Physics* (Cambridge University Press, Cambridge, England, 1990).
[35] L.B. Bezrukov and E.V. Bugaev, Yad. Fiz. **32**, 1636 (1980) [Sov. J. Nucl. Phys. **32**, 847 (1980)]; **33**, 1195 (1981) [**33**, 635 (1981)].
[36] J. Breitweg *et al.*, Eur. Phys. J. C **7**, 609 (1999).
[37] L.V. Volkova, G.T. Zatsepin, and L.A. Kuzmichev, Yad. Fiz. **29**, 1252 (1979) [Sov. J. Nucl. Phys. **29**, 645 (1979)].
[38] S. Higashi *et al.*, Nuovo Cimento A **43**, 334 (1966).
[39] DUMAND Collaboration, J. Babson *et al.*, Phys. Rev. D **42**, 3613 (1990).
[40] A. Okada, Astropart. Phys. **2**, 393 (1994).
[41] S. Miyake, in *Proceedings of the 13th International Conference on Cosmic Rays*, Denver, 1973 (Colorado Associated University, Boulder, 1973), Vol. 5, p. 3638.
[42] MACRO Collaboration, M. Ambrosio *et al.*, Phys. Rev. D **52**, 3793 (1995).
[43] V. M. Fedorov *et al.*, in *Proceedings of the 19th International Cosmic Ray Conference*, La Jolla, 1985, edited by F. C. Jones, J. Adams, and G. M. Mason, NASA Conference Publication 2376 (Goddard Space Flight Center, Greenbelt, MD, 1985), Vol. 8, p. 39.
[44] Yu.N. Vavilov *et al.*, Bull. Acad. Sci. USSR, Phys. Ser. (Engl. Transl.) **34**, 1759 (1970).
[45] V. A. Kudryavtsev (private communication).
[46] L. B. Bezrukov and E. V. Bugaev, in *Proceedings of the 17th International Cosmic Ray Conference*, Paris, 1981 (Section d'Astrophysique, Centre d'Études Nucléaires de Saclay, Gif-sur-Yvette Cedex, 1981), Vol. 7, p. 102; Yu.M. Andreev, L.B. Bezrukov, and E.V. Bugaev, Yad. Fiz. **57**, 2146 (1994) [Phys. At. Nucl. **57**, 2066 (1994)].
[47] S. R. Kelner, R. P. Kokoulin, and A. A. Petrukhin, Moscow Engineering Physics Institution Report No. 024-95, 1995; S.R. Kelner, R.P. Kokoulun, and A.A. Petrukhin, Yad. Fiz. **60**, 657 (1997) [Phys. At. Nucl. **60**, 576 (1997)].
[48] R. P. Kokoulin kindly granted us routines that had been written by him to compute muon cross sections. Some part of these routines are used in the MUM code.
[49] R.P. Kokoulin and A.A. Petrukhin, in *Proceedings of the 11th International Cosmic Ray Conference*, Budapest, 1969, edited by T. Gémsey *et al.* [Acta Phys. Acad. Sci. Hung. **29**, 277 (1970)]; R. P. Kokoulin and A. A. Petrukhin, in *Proceedings of the 12th International Cosmic Ray Conference*, Hobart, 1971, edited by A. G. Fenton and K. B. Fenton (University of Tasmania, Hobart, 1971), Vol. 6, p. A 2436.

[50] S.R. Kelner, R.P. Kokoulin, and A.A. Petrukhin, Yad. Fiz. **62**, 2042 (1999) [Phys. At. Nucl. **62**, 1894 (1999)].

[51] S. R. Kelner, Moscow Engineering Physics Institution Report No. 016-97, 1997.

[52] R.M. Sternheimer, Phys. Rev. **103**, 511 (1956); R.M. Sternheimer and R.F. Peierls, Phys. Rev. B **3**, 3681 (1971); R.M. Sternheimer, M.J. Berger, and S.M. Seltzer, At. Data Nucl. Data Tables **30**, 261 (1984).